Caveolin3 stabilizes McT1-mediated lactate/proton transport in cardiomyocytes

Peper J., Kownatzki-Danger D., Weninger G., Seibertz F., Pronto J.R., Sutanto H., Pacheu Grau D., Hindmarsh R., Brandenburg S., Kohl T., Hasenfuβ G., Gotthardt M., Rog-Zielinska E.A., Wollnik B., Rehling P., Urlaub H., Wegener J.W., Heijman J., Voigt N., Cyganek L., Lenz C., Lehnart S.E.

Circulation Research
2021 MAR 19 ; 128(6): e102-e120
2021 JAN 25 (first published online: final publication)
doi: 10.1161/CIRCRESAHA.119.316547

Publisher: American Heart Association | Lippincott Williams & Wilkins

Caveolin3 Stabilizes McT1-Mediated Lactate/Proton Transport in Cardiomyocytes

Jonas Peper[1,2,§], Daniel Kownatzki-Danger[1,2], Gunnar Weninger[1,2], Fitzwilliam Seibertz[3,4], Julius Ryan D. Pronto[3], Henry Sutanto[5], David Pacheu Grau[6], Robin Hindmarsh[2], Sören Brandenburg[1,2,4], Tobias Kohl[1,2,4], Gerd Hasenfuss[1,2,4,7], Michael Gotthardt[8,9,10], Eva A. Rog-Zielinska[11], Bernd Wollnik[7,12], Peter Rehling[6,7], Henning Urlaub[13,14], Jörg Wegener,[1,2,4] Jordi Heijman[5], Niels Voigt[3,4,7], Lukas Cyganek[2,4], Christof Lenz[13,14], Stephan E. Lehnart[1,2,4,7,15]

[1] Cellular Biophysics and Translational Cardiology Section, Heart Research Center Göttingen, and [2] Cardiology & Pneumology, University Medical Center Göttingen; [3] Institute of Pharmacology and Toxicology, University Medical Center Göttingen; [4] DZHK (German Centre for Cardiovascular Research), partner site Göttingen; [5]Cardiology, Cardiovascular Research Institute Maastricht, Maastricht University; [6] Cellular Biochemistry, University Medical Center, Georg-August-University; [7] Cluster of Excellence "Multiscale Bioimaging: from Molecular Machines to Networks of Excitable Cells" (MBExC), University of Göttingen; [8] Neuromuscular and Cardiovascular Cell Biology, Max Delbrück Center for Molecular Medicine in the Helmholtz Association, Berlin; [9]Cardiology, Virchow Klinikum, Charité - University Medicine, Berlin; [10] DZHK (German Center for Cardiovascular Research), partner site Berlin; [11] University Heart Center, Faculty of Medicine, University of Freiburg; [12] Institute of Human Genetics, University Medical Center Göttingen; [13] Bioanalytics, Institute of Clinical Chemistry, University Medical Center Göttingen. [14] Bioanalytical Mass Spectrometry, Max Planck Institute for Biophysical Chemistry, Göttingen, and; [15] BioMET, Center for Biomedical Engineering and Technology, University of Maryland School of Medicine, Baltimore, Maryland, USA.

[§] New affiliation: Institute of Developmental Biology and Neurobiology, Biozentrum I, Johannes-Gutenberg University Mainz, 55128 Mainz, Germany

Running title: Identification of McT1 as Caveolin3 Interactor

Subject Terms:
Basic Science Research
Cell Biology/Structural Biology
Ion Channels/Membrane Transport
Metabolism
Physiology

Address correspondence to:
Dr. Stephan E. Lehnart
Robert-Koch-Str. 42a
37075 Göttingen
Germany
Tel: +49 551-39-63631
slehnart@med.uni-goettingen.de

ABSTRACT

Rationale: Caveolin3 variants associated with arrhythmogenic cardiomyopathy and muscular dystrophy can disrupt post-Golgi surface trafficking. As Caveolin1 was recently identified in cardiomyocytes, we hypothesize that conserved isoform-specific protein/protein interactions orchestrate unique cardiomyocyte microdomain functions. To analyze the Caveolin1 versus Caveolin3 interactome, we employed unbiased live-cell proximity proteomic, isoform-specific affinity, and complexome profiling mass spectrometry techniques. We demonstrate the physiological relevance and loss-of-function mechanism of a novel Caveolin3 interactor in gene-edited human iPSC-cardiomyocytes.

Objective: To identify differential Caveolin1 versus Caveolin3 protein interactions and to define the molecular basis of cardiac CAV3 loss-of-function.

Methods and Results: Combining stable isotope labeling with proximity proteomics, we applied mass spectrometry to screen for putative Caveolin3 interactors in living cardiomyocytes. Isoform-specific affinity proteomic and co-immunoprecipitation experiments confirmed the monocarboxylate transporter McT1 versus aquaporin1, respectively, as Caveolin3 or Caveolin1 specific interactors in cardiomyocytes. Superresolution STED microscopy showed distinct Caveolin1 versus Caveolin3 cluster distributions in cardiomyocyte transverse tubules. CRISPR/Cas9-mediated Caveolin3 knock-out uncovered a stabilizing role for McT1 surface expression, proton-coupled lactate shuttling, increased late Na^+ currents, and early afterdepolarizations in human iPSC-derived cardiomyocytes. Complexome profiling confirmed that McT1 and the Na,K-ATPase form labile protein assemblies with the multimeric Caveolin3 complex.

Conclusions: Combining the strengths of proximity and affinity proteomics, we identified isoform-specific Caveolin1 versus Caveolin3 binding partners in cardiomyocytes. McT1 represents a novel class of metabolically relevant Caveolin3-specific interactors close to mitochondria in cardiomyocyte transverse tubules. Caveolin3 knock-out uncovered a previously unknown role for functional stabilization of McT1 in the surface membrane of human cardiomyocytes. Strikingly, Caveolin3 deficient cardiomyocytes exhibit action potential prolongation and instability, reproducing human reentry arrhythmias in silico. Given that lactate is a major substrate for stress adaption both in the healthy and the diseased human heart, future studies of conserved McT1/Caveolin3 interactions may provide rationales to target this muscle-specific assembly function therapeutically.

Keywords:
Caveolin3 knock-out; monocarboxylate transporter McT1; sodium channel Nav1.5; protein/protein interactions; Long-QT syndrome; metabolism; myocyte; mass spectrometry; human embryonic stem cells; mitochondria; interactum.

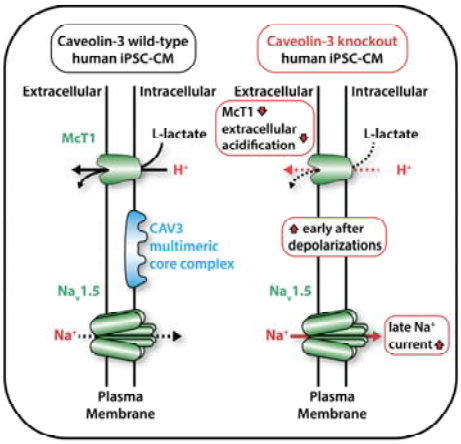

Nonstandard Abbreviations and Acronyms:

APEX2	Ascorbate peroxidase engineered X2 variant from soybean
AP-MS	Affinity purification mass spectrometry
BN-PAGE	Blue Native polyacrylamide gel electrophoresis
CAV1	Caveolin1
CAV3	Caveolin3
DDA-MS	Data-dependent acquisition mass spectrometry
DIA-MS	Data-independent acquisition mass spectrometry
EAD	Early after depolarization
$I_{Na,L}$	Late sodium current
KI	Knock-in
KO	Knock-out
LQTS9	Long-QT syndrome type 9
McT1	Monocarboxylate transporter type 1
$Na_V1.5$	Voltage-dependent Na^+ channel type 1.5
POI	Protein of interest
Src	Non-receptor protein tyrosine kinase
T-tubule	Transverse tubule
WT	Wild-type

INTRODUCTION

Cardiomyocytes exhibit a high density of caveolae in the plasma membrane increasing their surface area up to 2-fold.[1,2] Recent progress revealed how caveolae are molecularly stabilized through the coordinated actions of key lipid-binding proteins.[1] The partly membrane-integrated caveolin (CAV) family members CAV1 and CAV3, as well as Cavin1 were identified as essential cytosolic coat components that directly stabilize the characteristic omega-shaped caveolae structure in the surface membrane.[1,3] Moreover, the caveolar neck constriction is stabilized through a ring-shaped protein complex, where Eps15 homology domain 2 (EHD2) inhibits caveolar endocytosis.[3,4]

Since CAV1 knockout mice develop heart failure and CAV1 is abundant in fibroblasts, it was assumed that cardiomyocytes are not primarily affected.[5] In contrast, immuno-gold EM localized CAV1 in caveolae in human cardiomyocytes,[6] and immunoblotting demonstrated CAV1 expression in isolated mouse cardiomyocytes.[7] In addition, genome-wide studies have associated common CAV1 variants with cardiac conduction disease and atrial fibrillation.[8] Accordingly, a cardiomyocyte-specific mechanism of conduction disease was demonstrated in CAV1 knockout hearts.[7] However, neither the relationship between endogenous CAV1 and CAV3 nor human loss-of-function mechanisms were established in cardiomyocytes previously.

Both functionally important mechanoprotective and signal transduction roles have been assigned to caveolae.[1] For example, in skeletal muscle, flattening and disassembly of caveolae in response to increased stretch protects membrane integrity during muscle contraction.[2] In addition, G-protein coupled receptor and ion channel signaling have been associated with caveolae.[2,9] However, the multitude of candidate protein interactors cumulatively assigned through heterologous overexpression studies contrasts with recent observations in gene-edited cell lines showing that bulk membrane proteins are relatively depleted in caveolae.[10] Caveolar exclusion of membrane proteins was proposed to involve steric barriers provided by the coat and the ring protein complexes, as well as unfavorable membrane curvatures.[3,10] However, neither were putative CAV3 nor CAV1 binding proteins functionally established in cardiomyocytes.[1,2]

CAV1 knock-out mouse embryonic fibroblasts treated with dichloroacetate shift glucose utilization from lactate and pyruvate production to OXPHOS generation leading to cell death.[11] This was linked to mitochondrial dysfunction due to abnormal cholesterol accumulation leading to impaired mitochondrial import of the key antioxidant glutathione, such that OXPHOS increases reactive oxygen species (ROS) sufficiently to trigger apoptosis.[11] Notably, an increase in apoptotic hepatocytes and neurons was confirmed in CAV1 knockout mice in vivo.[11] Interestingly, in the failing human heart it has been shown that lactate is an important respiratory substrate and lactate uptake through McT1 is chronically increased, apparently compensating for decreased fatty acid utilization in mitochondrial energy production.[12] Finally, during exercise lactate uptake is markedly increased in cardiomyocytes and mitochondrial lactate oxidation may account for over 50% of oxygen consumption in the human heart.[12]

In patients, rare CAV3 variants cause a hypertrophic cardiomyopathy classified as long-QT syndrome type 9 (LQTS9).[9] Accordingly, overexpression of CAV3 containing the human F97C or S141R variants in HEK293 cells stably expressing the Na^+ channel $Na_V1.5$ resulted in increased late Na^+ currents.[9] On the other hand, CAV3 was found to co-purify with the dystrophin-glycoprotein complex (DGC) presumably through its interaction with nitric oxide synthase,[13] whereas $Na_V1.5$ was shown to bind to the DGC through α- and β-syntrophin.[14] Hence, the molecular nature of putative protein/protein interactions between the homomeric CAV3 core complex, $Na_V1.5$, DGC, and additional functional components remain unclear. As powerful live-cell proteomic and quantitative mass spectrometry techniques have emerged recently, we combined these to elucidate the spectrum of cardiac CAV1 and CAV3 protein interactions in an unbiased fashion.[15,16]

Here, we identify McT1 as a member of a new class of CAV3 binding proteins and a functional link to cardiac metabolism. While this interaction does not extend to the CAV1 isoform, McT1 and CAV3 occur in functionally important membrane domains, specifically in transverse (T-)tubules. In human iPSC-cardiomyocytes CAV3 knock-out uncovered a stabilizing role both for McT1 surface expression and co-transport of small monocarboxylates, particularly for lactate/proton shuttling. CAV3 knock-out significantly prolonged repolarization, leading to early afterdepolarizations (EADs), increased late sodium currents ($I_{Na,L}$), and computational modeling confirmed the proarrhythmic effects. While reciprocal co-immunoprecipitations do not support a stable CAV3 interaction with $Na_V1.5$ at endogenous levels in mature mouse cardiomyocytes, STED superresolution imaging showed these proteins clustered in T-tubules in proximity to each other. Complexome profiling enhanced by in-cell cross-linking confirmed a functional proximity of McT1, the Na,K-ATPase, and the Na/Ca-exchanger with the CAV3 complex in cardiomyocytes. Hence, stabilization of functional McT1 expression in the surface membrane requires isoform specific CAV3 protein interactions to sustain mitochondrial substrate exchange and electrical membrane stability.

METHODS

Data Availability.

The authors declare that all supporting data including complete protein tables are available within the article and the Data Supplement. More detailed methods are provided in the Data Supplement. The data that support the findings of this study are available from the corresponding author upon reasonable request. Please see the Major Resources Table in the Supplemental Materials.

Ratiometric APEX2 Proximity Assay by 3-State SILAC-MS.

We used the engineered peroxidase APEX2 to genetically tag CAV3 in living cardiomyocytes to label endogenous proteins in nanometric proximity of the macromolecular CAV3 complex via biotinylation (Figure 1A). Bicistronic recombinant adenoviral vectors were generated to express V5-APEX2-CAV3 and eGFP at the lowest effective multiplicity-of-infection (MOI 1) in neonatal rat ventricular myocytes

(NRCMs) for 48 h in culture (Table I in the Data Supplement). In addition, adenoviral V5-APEX2 expression served as soluble control. For ratiometric proteomic analysis we established 3-state SILAC (Stable Isotope Labeling by Amino Acids in Cell Culture) labeling in NRCMs (Figure 2A, Table II in the Data Supplement). Based on ≥96.5% SILAC incorporation after 13 days (Figure 2B), adenoviral transfection occurred on day 11 for subsequent V5-APEX2-CAV3 or V5-APEX2 protein labeling. Following H_20_2 treatment, differentially labeled cells were lysed and combined, and biotinylated proteins enriched by avidin. Avidin eluates were separated by SDS-PAGE into 12 fractions per lane, tryptically digested in-gel and identified by data-dependent acquisition mass spectrometry (DDA-MS) using a Top12 method on a hybrid quadrupole/orbitrap mass spectrometer (Q Exactive, Thermo Fisher Scientific) (Table III in the Data Supplement). Three independent SILAC cell cultures with label switches provided biological triplicates, each of which was analyzed by duplicate injections into the MS. Protein and peptide results were truncated to False Discovery Rates (FDR) of 1%, respectively. MS1 ion chromatograms were extracted using MaxQuant 1.5.7.4 software (Max Planck Institute for Biochemistry) and used for ratiometric protein quantitation (Detailed Methods in the Data Supplement).

CAV1/CAV3 Interactome Analysis by AP-DIA-MS.

For affinity purification-mass spectrometry (AP-MS), CAV1 and CAV3 were immunoprecipitated from 500 µg mouse ventricular tissues (Table IV and V in the Data Supplement). Eluted proteins were purified as a single fraction using 4-12% gradient gels and tryptically digested in-gel. Rabbit IgG (12-370, Merck) was used as negative control. Digested samples were analyzed on a hybrid quadrupole/time-of-flight mass spectrometer (TripleTOF 5600+, SCIEX). For generation of a spectral library a DDA-MS Top25 method was used and proteins identified using ProteinPilot 5.0 software (SCIEX). FDR was adjusted to 5% at this step. For quantitative analysis, data-independent acquisition mass spectrometry (DIA-MS) data were acquired using 65 variable size precursor windows across the 400-1,050 *m/z* range. Three biological replicates per sample were analyzed by triplicate injection into the MS. MS2 ion chromatograms for 6 fragments per peptide and up to 10 peptides per protein were extracted from the data using PeakView 2.1 software (SCIEX) to a False Detection Rate of 1%, and summed at the peptide and protein levels for statistical analysis (Detailed Methods in the Data Supplement).

Blue Native (BN)-PAGE Analysis, Co-immunoprecipitation, and Immunoblotting.

BN-PAGE was used to identify high molecular weight (MW) macromolecular complexes of the V5-APEX2-CAV3 fusion protein with endogenous CAV3 in NRCMs, as well as high MW complexes of recombinant wild-type (WT) or endogenous mouse CAV3 (Table VI and VII in the Data Supplement). Reciprocal co-immunoprecipitations followed by immunoblotting were used to confirm isoform specific CAV1 versus CAV3 protein interactions.

Complexome Profiling by BN-PAGE-MS.

Mouse ventricular cardiomyocytes were subjected to in-cell protein cross-linking using the homobifunctional cross-linker disuccinimidyl-suberate (DSS 0.1 mol/L, 1 h) to stabilize labile protein/protein complexes. Following lysis, proteins and protein/protein complexes were separated by BN-PAGE, visualized by Coomassie staining and cut into 23 equidistant gel fractions. Proteins were tryptically digested in-gel and analyzed by DDA-MS using a Top15 method on a hybrid quadrupole/orbitrap mass spectrometer (Q Exactive Plus, Thermo Fisher Scientific). Three biological replicates per sample were analyzed by duplicate injections into the MS. Protein and peptide results were truncated to False Discovery Rates (FDR) of 5%, respectively, to generate comprehensive candidate lists for hypothesis-driven data exploration. MS1 ion chromatograms were extracted using MaxQuant 1.5.7.4 software (Max Planck Institute for Biochemistry), combined to protein abundance values, normalized, and visualized as heat maps and line profiles (Detailed Methods in the Data Supplement).

Human CAV3 Knock-Out iPSC-Cardiomyocytes.

CRISPR/Cas9-mediated genome editing in human induced pluripotent stem cells (iPSCs) was applied to generate CAV3 knock-out lines, and engineered iPSCs were directly differentiated into ventricular-like

cardiomyocytes for functional analysis (Table IX through XI in the Data Supplement). The study was approved by the Ethics Committee (approval number 10/9/15) and carried out in accordance with approved guidelines.

Computational Modeling of Human iPSC-Cardiomyocytes.
Single-cell and tissue-level simulations were performed using the original Kernik human iPSC-cardiomyocyte model,[17] as well as a version prone to EAD development in the presence or absence of experimentally observed ion channel changes associated with CAV3 knock-out (Detailed Methods, Table XIII in the Data Supplement).

Statistical Analysis.
Data are presented as mean ± standard error of the mean (SEM) unless indicated otherwise. Unpaired 2-tailed Student's t-test or 1-way ANOVA was applied as specified in the figure legends. A p value <0.05 was considered as statistically significant (Detailed Methods in the Data Supplement).

RESULTS

Targeting the Macromolecular CAV3 Complex for Live-Cell Proteomics.

To label endogenous proteins in cardiomyocytes, we developed an N-terminally tagged V5-APEX2-CAV3 tool construct (Figure 1A). APEX2, an engineered peroxidase, is used to biotinylate proteins in nanometric proximity (i.e., ≤20 nm radius) to CAV3 in living cells upon H_2O_2 treatment for identification by affinity purification and mass spectrometric analysis of labeled proteins (Detailed Methods in the Data Supplement).[15,16] We hypothesized that V5-APEX2-CAV3 and endogenous CAV3 form a multimeric protein complex in neonatal rat cardiomyocytes (NRCMs) if their expression levels are similar. Using adenoviral vectors, we titrated the multiplicity of infection down to the lowest effective dose (MOI 1) and immunoblotting confirmed V5-APEX2-CAV3 expression levels similar to endogenous CAV3 (Figure 1B). Since plasmid-transfected NRCMs showed a significantly lower V5-APEX2-CAV3 expression (Figure 1B), we used adenoviral transfection of V5-APEX2-CAV3 (MOI 1) henceforth. As CAV3 expression in Sf9 cells produced a stable disc-shaped nonameric complex,[18] we asked if V5-APEX2-CAV3 is competent to bind endogenous CAV3 in a heteromeric complex?

Firstly, we used co-immunoprecipitation followed by V5 and CAV3 immunoblotting to exclude unspecific interactions with the soluble V5-APEX2 control. Supporting our hypothesis, co-immunoprecipitation of V5-APEX2-CAV3 confirmed endogenous CAV3 as binding partner (Figure 1C). Secondly, blue native (BN) gradient gel analysis showed a high MW complex under non-denaturating conditions. CAV3 immunoblotting confirmed a major complex at ~545 kDa both in untransfected and V5-APEX2-CAV3 transfected NRCMs (Figure 1D). In addition, V5 immunoblotting identified V5-APEX2-CAV3 unambiguously as exogenous component of the ~545 kDa complex (Figure 1D). To assess protein biotinylation in NRCMs qualitatively, we used avidin-affinity purification (Detailed Methods in the Data Supplement). This confirmed that V5-APEX2-CAV3 robustly labels endogenous proteins through biotinylation in living NRCMs treated for 1 min with H_2O_2 (Figure IA and IB in the Data Supplement). Finally, confocal imaging confirmed that V5-APEX2-CAV3 co-localizes with endogenous CAV3 in NRCMs (Figure 1E; for MOIs >1 see Figure IC in the Data Supplement).

Quantitative CAV3 Proximity Proteomics in Cardiomyocytes.

To develop a quantitative proteomic approach, we established a 3-state SILAC workflow for systematic label switching (Figure 2A; Figure IIA in the Data Supplement). NRCMs cultured in SILAC media expressing V5-APEX2-CAV3 showed ≥96.5% isotope label incorporation (Figure 2B). As

ratiometric controls, we used adenoviral transfections of V5-APEX2 and eGFP based on published protocols.[16,19] V5-APEX2-CAV3 and V5-APEX2 expression was confirmed by V5 immunoblotting (Figure 2C). Biotinylated proteins were enriched by affinity purification and AP-MS identified 1131 biotinylated proteins, of which 101 proteins including 9 proteins of interest (POIs) were significantly enriched for V5-APEX2-CAV3 (Figure 2D, dataset Excel Table I in the Data Supplement). As expected for CAV3 protein complexes assembled in the ER and Golgi followed by vesicular trafficking to the surface membrane, V5-APEX2-CAV3 labeling occurred in the proximity of different organelles, for example in ER-associated mitochondria (Figure IIB in the Data Supplement).[11] Electron tomography confirmed that caveolae are situated in less than 10 nm proximity to mitochondria in cardiomyocytes (Figure IIC through IIE, Table VIII in the Data Supplement), and, thus, within the expected 20 nm radius of the reactive V5-APEX2-CAV3 generated biotin labeling cloud.[15,16]

Using the STRING protein/protein interaction database[20] we mapped the interaction networks of the identified POIs using the GO terms 'caveolae', 'muscle contraction', 'pyruvate metabolism', and 'iron uptake & transport' (Figure 2E). Confirming our proximity proteomic strategy, all essential and muscle-specific components of the core caveolar complex, namely CAV3, Cavin1 and Cavin4 were identified consistent with earlier studies.[21,22] Surprisingly, we identified CAV1, while Pacsin2 has been associated with caveolae previously.[23] Moreover, myosin light chain (Myl2, Myl3, Myl6), actin (Acta1, Acta2 and Actc1), and troponin (Tnni1) were identified together with the Na,K-ATPase α1 and β1 subunits, and the Na/Ca exchanger (Ncx1) confirming earlier studies.[24,25] Finally, proteins that define key transmembrane metabolic substrate carriers were detected (dataset Excel Table I in the Data Supplement). Importantly, we identified the monocarboxylate transporter McT1 and the transferrin receptor TfR1 as new CAV3 proximity candidates (Figure 2E).

Differential CAV1 versus CAV3 Expression in Cardiomyocytes.

As the presence of CAV1 in striated muscle cells remains controversial,[5,26] we validated CAV1 protein expression in lysates of ventricular cardiomyocytes isolated from adult mouse hearts. Immunoblotting confirmed that CAV1 is robustly expressed, visible as a single band below 25 kDa, while antibody specificity was confirmed in CAV1 knock-out mouse hearts (Figure 3A; Figure IIIA in the Data Supplement). Moreover, label-free data-independent acquisition mass spectrometry (DIA-MS) established the expression of all three mammalian CAV isoforms in isolated cardiomyocytes, surprisingly with the highest protein area measured for CAV1 (Figure 3B, dataset Excel Table II and III in the Data Supplement). DIA-MS protein areas were previously demonstrated to correlate strongly with absolute cellular protein concentrations even without the use of quantified standards.[27] Out of 1816 proteins detected, the ubiquitous CAV1 isoform was ranked #205 by protein area and thus highly abundant, whereas the muscle-specific CAV3 ranked #1105 indicating a much lower abundance (Figure 3C).

To investigate the relationship between CAV1 and CAV3 in adult ventricular cardiomyocytes, we used confocal and STimulated Emission Depletion (STED) superresolution microscopy (nanoscopy). STED nanoscopy resolved CAV1 cluster signals in physiologically relevant membrane structures, namely the intercalated disk and T-tubules, but not in the lateral surface membrane (Figure 3D). While the CAV1 and CAV3 signals occurred frequently adjacent to each other in T-tubules, STED did not resolve co-localized signals (Figure 3D). Unspecific CAV1 signals in T-tubules were excluded using murine CAV1 knockout cardiomyocytes as negative control (Figure IIIB in the Data Supplement). Finally, reciprocal immunoprecipitation of CAV1 versus CAV3 in cardiomyocyte lysates indicated relatively weak heteromeric versus strong homomeric protein interactions (Figure 3E). Hence, CAV1 and CAV3 clusters are differentially distributed in cardiomyocytes, presumably each in isoform-specific homomeric core complexes, but frequently positioned near each other in T-tubule nanostructures.

Isoform-Specific CAV Interactions.

To explore the hypothesis that CAV1 and CAV3 provide macromolecular scaffolds for differential subcellular protein interactions, we analyzed mouse ventricular tissue lysates by immunoprecipitation followed by quantitative DIA-MS. CAV1 and CAV3 were readily differentiated by the detection and quantification of multiple isoform-specific peptides following tryptic digestion of immunoprecipitation eluates (Figure IVA and IVB, dataset Excel Table II and III in the Data Supplement). We detected 62 potential protein interactions for CAV1 (Figure VA in the Data Supplement) and 70 for CAV3 (Figure VB in the Data Supplement) using permutation-based false discovery rate analysis ($p<0.05$).[28] To identify isoform-specific interactions, we compared the respective CAV1/CAV3 enrichment ratios and found 7 interactors specific for CAV1 versus 23 for CAV3 (Figure 4A). Importantly, among POIs with an established pathophysiological role, affinity-based DIA-MS confirmed McT1 as a previously unknown CAV3 interactor (Figure 4A). Next, we compared the fold change of the logarithmic ratio each for CAV1 or CAV3 normalized to IgG (Figure 4B), confirming preferential CAV1 interactions with aquaporin-1, CAV1, CAV2, Cavin1 and Cavin2. In contrast, CAV3 binds preferentially to itself, the insulin-dependent glucose transporter GluT4, to McT1, the Na,K-ATPase α1 and β1 subunits, Connexin43, and Ncx1. Consistent with the concept of preferential homomeric isoform-specific complexes, significant heteromeric interactions between CAV1 and CAV3 were not detected by affinity-based DIA-MS (Figure 4B).

To validate our findings, we performed reciprocal immunoprecipitation experiments followed by immunoblotting in mouse ventricular tissue lysates. Whereas CAV1 showed an exclusive interaction with aquaporin1, we confirmed isoform specific CAV3 interactions with connexin43, McT1, and TfR1. Again, relatively weak heteromeric interactions between CAV1 and CAV3 were evidenced, contrasting with strong homomeric self-interactions (Figure 4C). Finally, STED nanoscopy resolved McT1 clusters as punctate signals both in the lateral surface membrane and in T-tubules of adult mouse cardiomyocytes, and consistent with differential subcellular CAV3 versus CAV1 distributions (Figure 4D). As small McT1 clusters were frequently localized on the edge or inside CAV3 clusters, we propose that McT1 is functionally associated with CAV3 complexes in the plasma membrane. Taken together, these data confirm isoform-specific protein interactions of CAV3 with McT1 and highlight their physiologically relevant location in T-tubules in nanometric proximity to mitochondria (Figure IID and IIE in the Data Supplement).

CAV3 Knockout Affects McT1 Surface Expression in Human Cardiomyocytes.

We hypothesized that protein/protein interactions with the CAV3 complex stabilize functional McT1 expression in the surface membrane. To test this, we generated a human induced pluripotent stem cell (iPSC) knock-out model (CAV3 KO) targeting the start codon of exon 1 by CRISPR/Cas9 (Figure VI in the Data Supplement). Immunoblotting of ventricular-like cardiomyocyte lysates derived from WT iPSC confirmed robust expression of CAV3 and McT1 (Figure 5A). In contrast, CAV3 KO iPSC-cardiomyocytes (iPSC-CMs) were completely CAV3 deficient, whereas McT1 protein expression was decreased (Figure 5A). To explore if the McT1 decrease is functionally relevant in the sarcolemma, we applied extracellular surface biotinylation to living cardiomyocytes in culture. Surface biotinylated proteins were enriched by pull-down and McT1 identified by immunoblotting. Indeed, McT1 was specifically decreased in the surface membrane of CAV3 KO cardiomyocytes (Figure 5B).

To investigate if decreased McT1 surface expression functionally impacts substrate uptake, we exposed human iPSC-CMs to extracellular 3-bromopyruvate (3-BP), a glycolysis-disrupting compound previously established as McT1-specific substrate.[29,30] Accordingly, WT and CAV3 KO cardiomyocytes were treated with 3-BP (50 µmol/L) and cell viability was assessed by lactate dehydrogenase (LDH) release using published protocols.[31] Consistent with McT1 loss in the surface membrane leading to decreased 3-BP uptake, LDH release was significantly decreased in human CAV3 KO iPSC-CMs (Figure 5C).

McT1 is thought to represent the major pathway for transmembrane lactate and pyruvate transport in the heart,[32] and is upregulated in heart failure.[12] To assess if human CAV3 KO cardiomyocytes experience substrate-dependent metabolic limitations, we measured oxygen consumption and extracellular acidification using Seahorse protocols established for iPSC-CMs previously (Table XI in the Data Supplement).[33] While oxygen consumption was normal in CAV3 KO cardiomyocytes (Figure 5D), extracellular acidification was significantly decreased (Figure 5E). Moreover, inhibiting ATP synthesis with oligomycin increased extracellular acidification maximally in WT but not in CAV3 KO cardiomyocytes consistent with impaired proton-coupled lactate export (Figure 5E). Finally, mitochondrial uncoupling by ionophore (FCCP) or electron transport chain inhibition (Antimycin+Rotenone) did not result in further changes. Together, these experiments established that CAV3 KO destabilizes functional McT1 surface expression and extracellular acidification through the lactate/proton shuttle in human iPSC-CMs.

CAV3 Deficiency Increases Action Potential Duration (APD) and Promotes Early Afterdepolarizations (EADs).

Based on optical recording of spontaneous iPSC-CM depolarizations using the voltage-sensitive dye FluoVolt (final kit dilution 0.1x according to manufacturer instructions; Detailed Methods in the Data Supplement), action potentials from CAV3 KO compared to WT cells showed a profound delay of repolarization (Figure 6A). Both individual and averaged APD values at 50% and 90% of repolarization (APD_{50} and APD_{90}) were significantly prolonged in CAV3 KO iPSC-CMs (Figure 6B).

In addition to APD prolongation, the relationship between early and late repolarization given by the repolarization fraction ($[APD_{90} - APD_{50}]/APD_{90}$) was significantly increased in CAV3 KO iPSC-CMs (Figure 6C). This indicates that CAV3 KO may not only delay repolarization but promote beat-to-beat electrical instability. Indeed, spontaneously generated action potentials were followed by singular as well as repetitive (regenerative) APDs (Figure 6D). On average, in the absence of any pharmacological interventions 35% of the human CAV3 KO cells produced EADs in sharp contrast to 0% of the WT control iPSC-CMs (Figure 6E). As human CAV3 variants associated with LQTS9 were shown to increase late Na^+ currents after overexpression in HEK293 cells,[9] we aimed to confirm the putative $Na_V1.5$ channel interaction under physiological conditions in iPSC-CMs.

Whole-cell patch-clamp measurements showed similar Na^+ current (I_{Na}) behaviors in WT and CAV3 KO iPSC-CMs throughout step-wise depolarizations (Figure 6F, left). Comparing current density-voltage relations between WT versus CAV3 KO showed no difference, particularly no significant change of the peak I_{Na} (Figure 6F, right). However, an increased TTX-sensitive $I_{Na,L}$ was observed in CAV3 KO iPSC-CMs (Figure 6G, left). Accordingly, the calculated $I_{Na,L}$ integral confirmed a significant $I_{Na,L}$ increase in human CAV3 KO iPSC-CMs (Figure 6G, right).

Proximity proteomics has identified both Na,K-ATPase subunits near CAV3 (Figure 2). However, direct Na,K-ATPase interactions through a binding motif, essential for organogenesis, were recently established only for CAV1.[34] Patch-clamp recording in WT versus CAV3 KO iPSC-CMs showed similar activation and inhibition of Na,K-ATPase currents following 5 mmol/L extracellular K^+ or 10 µmol/L ouabain, respectively (Figure VIIA and VIIB, Table XII in the Data Supplement). Accordingly, activation followed by inhibition of the Na,K-ATPase pump did not reveal any significant current differences in CAV3 KO iPSC-CMs (Figure VIIC in the Data Supplement). Taken together, CAV3 KO leads to decreased lactate/proton extrusion, increased late $I_{Na,L}$ currents, and APD prolongation with EAD instability in iPSC-CMs.

We employed computational modeling to investigate the specific contribution of $I_{Na,L}$ to EAD generation and tissue-level proarrhythmic consequences. At baseline, the WT iPSC-CM model does not have an appreciable $I_{Na,L}$ consistent with our WT experimental data, while incorporating the increased $I_{Na,L}$ associated with CAV3 KO (Figure VIII, Table XIII in the Data Supplement) produced a minor APD

prolongation (Figure 6H, EAD-resistant cell). However, models prone to EAD development due to additional changes in $I_{Ca,L}$ and reduced repolarization reserve, based on experimental data,[35,36] had a significantly longer baseline APD and developed runs of EADs in the presence of $I_{Na,L}$ upregulation (Figure 6H, EAD-prone cell), thus resembling the electrophysiological phenotype observed in CAV3 KO iPSC-CMs (Figure 6A through 6E).

Incorporating a mix of EAD-resistant and EAD-prone cells in two-dimensional tissue simulations revealed their proarrhythmic potential. In the presence of a sufficiently large area of EAD-prone cells, tissue simulations exhibited (repetitive) focal activity (Figure IX, Video I in the Data Supplement). Moreover, under specific conditions (involving the location of EAD-prone cells relative to the normal activation wave front and the APD of EAD-prone cells), EAD-prone cells can also elicit a figure-of-eight reentry pattern (Figure 6I, Figure X, Video II in the Data Supplement), confirming the proarrhythmic phenotype observed in CAV3 KO cells at the tissue level in silico.

CAV3 Does not Co-immunoprecipitate or Co-localize with $Na_V1.5$ Channels.

Using a caveolin-rich rat cardiomyocyte membrane fraction for CAV3 immunoprecipitation, immunoblotting suggested the cardiac Na^+ channel as associated protein.[37] When WT CAV3 was overexpressed with human $Na_V1.5$ in HEK293 cells, immunoblotting after CAV3 immunoprecipitation indicated a similar protein association.[9] However, the reciprocal $Na_V1.5$ immunoprecipitation confirming CAV3 as putative interaction partner was not established.

Firstly, using the protocol of Vatta et al[9], CAV3 versus CAV1 were immunoprecipitated in WT mouse ventricular lysates followed by $Na_V1.5$ immunoblotting. While the Na^+ channel was confirmed in the input fraction, $Na_V1.5$ was not detected after immunoprecipitation (Figure XIA in the Data Supplement), while strong isoform-specific CAV1 and CAV3 self-interactions were confirmed (Figure XIB in the Data Supplement).

Secondly, we used a cardiac-restricted double-transgenic model expressing human FLAG-$Na_V1.5$ to immunoprecipitate the protein via FLAG-antibody in mouse heart lysates.[38] Immunoblotting confirmed human FLAG-$Na_V1.5$, mouse $Na_V1.5$, and CAV3 in the input fraction (Figure 7A). Following anti-FLAG immunoprecipitation, immunoblotting confirmed both the FLAG and human $Na_V1.5$, whereas mouse $Na_V1.5$ was not detected (Figure 7A). While CAV3 was abundantly present (input), however, CAV3 was not detected after human FLAG-$Na_V1.5$ immunoprecipitation (Figure 7A).

Thirdly, using a protocol that supports co-immunoprecipitation of the PDZ domain-binding protein SAP97 together with $Na_V1.5$ by Milstein et al[39], we tested the putative CAV3 interaction in WT mouse ventricular lysates. Whereas immunoblotting identified $Na_V1.5$ and SAP97 (positive control) after immunoprecipitation, rabbit IgG served as negative control. However, while CAV3 was present (input), only the direct $Na_V1.5$ interactor SAP97 but not CAV3 were detected (Figure 7B).

Finally, since co-localization of CAV3 and $Na_V1.5$ both in human and rat hearts has been reported previously,[9,37] we performed high-resolution confocal and STED imaging studies in mouse cardiomyocytes. Interestingly, confocal imaging frequently showed yellow signal spots in transversal striations suggesting that CAV3 and $Na_V1.5$ may be co-localized in T-tubules (Figure 7C). In contrast, by switching on the STED laser beam, CAV3 versus $Na_V1.5$ signals were resolved as spatially separate clusters in T-tubule striations, but apparently not co-localized (Figure 7C). Hence, neither co-immunoprecipitation nor co-localization, consistent with proximity- and affinity-based MS, can support the previously proposed interaction between $Na_V1.5$ and CAV3 at physiological protein levels in mature mouse cardiomyocytes.

Complexome Profiling Confirms Labile Protein Assemblies with the CAV3 Complex.

To resolve the association of multimeric CAV3 complexes with McT1 and cardiac ion transport complexes according to apparent weight, we used BN-PAGE separation followed by mass spectrometry (BN-PAGE-MS). Untreated versus DSS treated (0.1 mmol/L, 1 h) mouse ventricular cardiomyocytes were analyzed to test if in-cell cross-linking enhances the detection of labile protein/protein complexes (Methods, Detailed Methods in the Data Supplement). Protein complexes of membrane fractions each from untreated and DSS treated cells were separated on BN-PAGE gradient gels (Figure XIIA in the Data Supplement). Each BN-PAGE lane was cut into 23 equally sized slices for in-gel tryptic digestion and data-dependent acquisition MS (DDA-MS). For mass calibration, we used a standard set of membrane proteins and protein complexes following protocols established previously (Figure XIIB in the Data Supplement).[40] 2460 proteins were reproducibly detected in both conditions (Figure XIIC, dataset Excel Table IV in the Data Supplement). Normalized BN-PAGE-MS intensity mapping identified the CAV3 complex at an apparent weight of ≥300 kDa in untreated cardiomyocytes (Figure 8A). Interestingly, McT1, the Na,K-ATPase α1/β1, Ncx1, and TfR1 were detected nearby at 100-300 kDa (Figure 8A). Abundance line profiling confirmed that the CAV3 complex abundance peak was clearly separated in mass from the McT1, Na,K-ATPase α1, and Ncx1 peaks with minimal overlap in the 100-400 kDa range (Figure 8B).

While the abundance pattern was similar for the CAV3 complex following live-cell DSS cross-linking (0.1 mmol/L), apparently McT1, Na,K-ATPase α1/β1, Ncx1, and TfR1 were shifted leftward towards the 100-400 kDa range (Figure 8C). Line profile plots confirmed that DSS cross-linking resulted in left-shifted major abundance fractions and additional minor peaks each for McT1, Na,K-ATPase α1, and Ncx1, overlapping with the CAV3 complex (Figure 8D). As DSS cross-linking captures proteins in direct proximity due to the restricted length of the cross-linker, McT1, the Na,K-ATPase, and Ncx1 may form labile protein assemblies with the CAV3 isoform complex, stabilizing electro-metabolic transport functions in a highly localized fashion in cholesterol-rich microdomains in cardiomyocytes.

DISCUSSION

Combining the strengths of proximity- and affinity-based proteomics, we have identified previously unknown, isoform-specific CAV1 versus CAV3 protein interactions in cardiomyocytes. Reciprocal co-immunoprecipitation experiments confirmed McT1 and TfR1 as new CAV3-specific binding partners of immediate relevance for cardiac metabolism and aquaporin1 as a CAV1-specific interactor. Surprisingly, quantitative proteomics identified CAV1 as a highly abundant isoform in cardiomyocytes relative to less abundant muscle-specific CAV3. Consistent with a functionally important and CAV3-dependent McT1 interaction in the surface membrane, CAV3 knock-out uncovered a stabilizing role for transmembrane lactate/proton shuttling in human cardiomyocytes. Moreover, CAV3 knock-out is sufficient to significantly increase $I_{Na,L}$ leading to delayed AP repolarization and EADs in iPSC-CMs, and arrhythmias in mathematical iPSC-CM and tissue models, reminiscent of the human CAV3 variant LQTS9 phenotype in patients. At endogenous CAV3 and $Na_V1.5$ protein levels in mouse hearts a functional association in T-tubules may occur through nanometric cluster proximities, while two independent co-immunoprecipitation approaches exclude stable protein interactions. Importantly, while we established the first physiological human iPSC-CM CAV3 KO model exhibiting McT1 surface destabilization and electro-metabolic dysfunction, complexome profiling confirmed labile protein assemblies of McT1, the Na,K-ATPase, and Ncx1 with the CAV3 complex in living adult mouse cardiomyocytes. While a constitutive McT1 surface expression in cardiomyocytes was proposed previously,[41] our data define the CAV3 complex as a muscle-specific protein interaction hub with major implications for cardiac cell biology, local electro-metabolic transmembrane transporter organization, and specific CAV3 loss-of-function phenotypes.

STED nanoscopy showed that CAV3 and McT1 are frequently co-clustered in the lateral cardiomyocyte surface membrane and in T-tubules. Immunogold EM studies demonstrated previously that McT1 is highly abundant in caveolae, the intercalated disks, and T-tubules, but only the latter showed dense immunogold labeling in direct proximity to mitochondria.[41] While this suggests a privileged McT1-mitochondrial metabolite shuttling pathway at T-tubules, we identified CAV3 as an isoform-specific interactor of McT1. CRISPR/Cas9 knock-out in human cardiomyocytes established a causal functional role, since McT1 expression was specifically decreased in the plasma membrane of CAV3 deficient cells. McT1 is known to facilitate the proton-coupled transport of small monocarboxylates, most importantly of lactate and pyruvate.[32] During exercise lactate represents a major cardiac energy source that may account for over 50% of oxygen consumption.[42] Whereas cardiac ischemia drives lactate efflux from affected cells,[43] chronic heart failure leads to significantly increased McT1 protein expression and lactate uptake.[12]

Given that McT1 has a prominent role in cardiac stress adaptation, our discovery that CAV3 interacts with McT1, functionally stabilizes substrate metabolism, and electrical membrane stability in human cardiomyocytes is highly relevant for the healthy and diseased heart. As cultured iPSC-derived cardiomyocytes predominantly utilize glucose for ATP production,[44] energy homeostasis depends directly on McT1 surface expression and proton-coupled metabolite export.[32] Consistent with this model CAV3 knock-out resulted in significantly decreased extracellular acidification. Interestingly, pharmacologic inhibition of monocarboxylate transport in tumor cells rapidly increases intracellular lactate, whereas ATP and glutathione (GSH) synthesis are decreased, contributing to mitochondrial dysfunction.[45]

Quantitative proteomics and superresolution imaging established that CAV1 is highly abundant in the intercalated disks and T-tubules in adult mouse cardiomyocytes. Our data thus overcomes the prevailing notion that CAV1 is expressed predominantly in non-muscle cells.[1] In addition, immunolabeling freeze-fracture EM studies localized CAV1 in caveolae of human heart sections previously.[6] Here, STED nanoscopy showed that CAV1 and CAV3 are not co-localized, although clusters of the two isoforms occurred frequently adjacent to each other in T-tubules. This supports the new hypothesis of isoform-specific subcellular nanodomain functions based on unique protein interactions of CAV1 versus CAV3 complexes. While an in-depth analysis of the CAV1 complex and confirmation of aquaporin1 as a newly identified candidate interactor remain important questions for future studies, our findings offer a new cell biological perspective. CAV3 does not function as predominant but rather as additional muscle-specific isoform to locally stabilize and augment a unique set of essential metabolic functions (i.e., McT1, Ncx1, Na,K-ATPase transport in T-tubules in proximity to mitochondria). Vice versa, the historic notion that CAV1 has no role in cardiomyocytes needs careful re-investigation. As CAV1 is highly abundant in mature mouse cardiomyocytes, it seems unlikely that CAV1 knock-out mice develop heart failure mainly from fibroblast defects.[5] Furthermore, our findings have important implications for patients with CAV1 or CAV3 variants.

In line with our proteomic data (Figure 4A and 4B), the CAV3 variant P104L associated with limb girdle muscular dystrophy was shown to diminish insulin-induced surface expression of GluT4 and glucose uptake in skeletal myotubes.[46] Interestingly, Golgi accumulation and mechanosensing defects were recently demonstrated for the CAV3 variants P28L and R26Q in skeletal myofibers of patient biopsies.[47] This raises the possibility that pathogenic CAV3 variants affect both the heart and skeletal muscles through multi-factorial defects including i) Golgi accumulation and protein-lipid aggregation; ii) disrupted surface trafficking and iii) cholesterol surface transport leading to mitochondrial toxicity;[11] iv) local metabolic substrate transport via Glut4[46] and McT1;[48] v) local electrophysiologically important ion transport interactions with Nav1.5 (Figure 6A through 6I, Figure 7C), and putatively with Ncx1[25]; vi) mechano-protective membrane plasticity;[2] and vii) mechanosensing.[47] Additionally, CAV3 may interact with the angiotensin II receptor (AT1R) during exocytic transport, whereas the human CAV3-P104L variant disrupts AT1R surface trafficking.[49] Moreover, CAV3 knock-out in mice induces hypertrophy and cardiomyopathy, whereas cardiomyocyte-restricted CAV3 overexpression attenuated cardiac hypertrophy.[50] Finally, while the CAV1 variant P132L was associated with extracardiac pathologies, CAV1-P132L overexpression

resulted in Golgi accumulation.[51] Taken together, our findings of isoform-specific protein interactions provide a template for future studies to determine pathogenic CAV3 mechanisms as well as the currently unknown impact of a large spectrum of human CAV1 variants in the context of cardiac and skeletal muscle dysfunction.

CAV1 knockout in mice has been shown to decrease left-ventricular conduction velocity through decreased connexin43 expression.[7] As STED imaging showed few residual CAV1 signals in CAV1 KO mouse cardiomyocytes at the intercalated disc but not in T-tubules, we have to assume some unspecific local antibody binding. Nonetheless, we confirmed robust CAV1 expression in mouse cardiomyocytes by immunoblotting in WT versus CAV1 KO mouse cardiomyocytes and quantitatively by DIA-MS in mouse ventricles. Importantly, our proteomic analysis showed isoform–specific CAV3 interactions with connexin43 and Ncx1, whereas aquaporin1 was confirmed as a CAV1-specific interactor through co-immunoprecipitation experiments. While human CAV1 and CAV3 are 61% identical, only CAV1 exhibits an extended N-terminal domain subject to Src phosphorylation at tyrosine-14, augmenting Src binding to CAV1.[52] As the CAV1 variant P132L represents a well-established model of disrupted caveolae biogenesis,[51] follow-up studies will need to explore the impact of this particular human variant and putative aquaporin1 interactions in cardiomyocytes.

Excessive overexpression in heterologous cell systems has been shown to interfere with caveolae biogenesis, to lead to aberrant CAV1 trafficking, and to increase the pool of ectopic non-caveolar CAV1.[51,53] For example, 4 hours after CAV1 transfection in fibroblasts most of the overexpressed CAV1 failed to co-localize with endogenous CAV1 in caveolae, instead accumulating in the late endosome.[54] Notably, overexpression of V5-APEX2-CAV3 at an MOI ≥3 resulted in Golgi aggregates in NRCMs. Therefore, we have carefully titrated adenoviral expression of V5-APEX2-CAV3 to the lowest effective dose, demonstrating a similar distribution as endogenous CAV3 indicative of preserved CAV3 surface trafficking. Consistent with proteomic toxicity and our observations, 3-fold transgenic overexpression of WT CAV3 causes a degenerative cardiomyopathy in mice with severely diminished sarcolemmal dystrophin expression.[55]

Genome editing of NIH3T3 cells enabled CAV1 expression at low endogenous levels, demonstrating recently that caveolae are endocytosed at a very low rate, while bulk membrane proteins are effectively excluded from caveolae.[10] In contrast, earlier studies used quantitatively uncontrolled overexpression of LQTS9 associated CAV3 variants in HEK293 cells to infer ectopic interactions with human $Na_V1.5$ increasing $I_{Na,L}$ currents.[9] Affinity- and proximity-based proteomic analysis did not detect $Na_V1.5$ as putative CAV1 or CAV3 interactor in rodent cardiomyocytes. However, human CAV3 KO iPSC-CMs revealed ~2-fold increased $I_{Na,L}$ contributing to EAD instability, a directly proarrhythmogenic mechanism confirmed in mathematical iPSC-CM and tissue modeling by focal and reentry-type arrhythmias. Two independent, reciprocal CAV3 versus $Na_V1.5$ co-immunoprecipitation approaches failed (based on the same protocols published previously[9,39]) to confirm the ectopic interaction observed in HEK293 cells possibly due to the lower physiological protein levels. However, STED nanoscopy showed that CAV3 and $Na_V1.5$ clusters exist frequently in nanometric proximity to each other in T-tubules of mouse cardiomyocytes, supporting a local functional interaction, without co-localization as reported previously by light diffraction-limited confocal imaging.[9] Hence, our observation that CAV3 KO destabilizes lactate/proton shuttling and causes electrical instability in human iPSC-CMs introduces a novel loss-of-function and a unifying disease model relevant for follow-up studies of trafficking-incompetent CAV1 and CAV3 variants.

Study limitations.

The proximity proteomic analysis used immature NRCMs and CAV3 KO occurred in immature human iPSC-CMs, which may not translate to the adult situation. Therefore, we applied an in-depth multiplexed strategy followed by immunoprecipitation AP-MS and co-immunoprecipitation experiments to

confirm or reject candidate CAV3 interactors in adult mouse heart lysates. Data from the ratiometric APEX2 proximity assay were searched against *Rattus norvegicus* UniProtKB database. While it is not complete with regard to cardiac proteins, we consciously chose not to use a combined murine database to avoid ambiguities by protein entry mapping. In addition, complexome profiling confirmed labile protein assemblies in adult mouse cardiomyocytes. Finally, subcellular in situ analysis of McT1, $Na_V1.5$, CAV1, and CAV3 cluster locations by confocal and STED imaging was performed in adult mouse cardiomyocytes, and nanodomain proximities of caveolae at the surface and intracellular T-tubules with mitochondria were confirmed by Electron Tomography.

For a majority of proteins information regarding their participation in functionally important macromolecular complexes is still lacking. For this purpose, we employed an optimized approach for complexome profiling comprising BN-PAGE separation and mass spectrometry, enhanced by in-cell cross-linking to stabilize labile interactions otherwise lost during analysis. This confirmed a labile protein assembly of McT1, Ncx1, and the Na,K-ATPase with the CAV3 complex in cardiomyocytes. In summary, we applied APEX2 proximity proteomics identifying McT1 as putative CAV3 interactor in NRCMs. As a second isoform-specific approach, AP-MS was used to establish CAV1- versus CAV3-specific interactors. For CAV3 we identified McT1 and TfR1 as novel isoform-specific interactors relevant for cardiac energy metabolism, whereas aquaporin1 was identified for CAV1. Hence, combining proximity and affinity proteomics, we demonstrate that previously unknown and canonical interactors of CAV complexes can be detected with high specificity, providing a comprehensive strategy for systematic functional analysis. Furthermore, we show that McT1, an abundant cardiac lactate/proton co-transporter, requires CAV3 for stable functional surface expression in human cardiomyocytes. In contrast, CAV3 KO disrupted McT1-dependent substrate-transport, increased $I_{Na,L}$ leading to EAD instability in human cardiomyocytes, and proarrhythmogenic reentry in iPSC-CM tissue modeling. These observations highlight the potential of in situ protein labeling and cross-linking approaches to identify new interaction partners and structural interfaces for CAV1 or CAV3 multimers, which are prerequisites to generate assembly models of functional protein complexes in the physiological context of excitable cells. Hence, characterization of novel interactors of CAV1 and CAV3 complexes is central to understand their isoform-specific functions in cardiac cell biology, and to develop therapeutic rationales that exploit conserved protein/protein interfaces to augment McT1 function, or to inhibit $I_{Na,L}$ causative EAD instability in heart disease.

ACKNOWLEDGMENTS
We are grateful for excellent technical assistance by Birgit Schumann, Brigitte Korff, Laura Cyganek, Lisa Neuenroth, Thierry Wasselin, Nadine Gotzmann, Martina Grohe, Yvonne Hintz, Lisa Krebs and Yvonne Wedekind; to Steven O. Marx for kindly providing FLAG-$Na_V1.5$ expressing transgenic mice; to Carolin Wichmann for high-pressure freezing and sample preparation for electron tomography; and to Martin Schorb from the Electron Microscopy core facility at the EMBL Heidelberg.

SOURCES OF FUNDING
This project was funded by Deutsche Forschungsgemeinschaft (DFG) collaborative research units SFB1002 to SEL (projects A09 and S02), to PR (project A06), to NV (project A13), to GH (project D01), to BW (D02), to LC (project S01); and through SFB1190 to SEL (project P03), and to HU (project Z02); and was supported under Germany's Excellence Strategy (EXC2067/1-390729940). NV was funded by Deutsche Forschungsgemeinschaft (VO15568/3 and IRTG1816 RP12.3) and the Else-Kröner-Fresenius Foundation (EKFS 2016_A20). SB received financial support through the clinician scientist program "Translational Medicine" of the University Medical Center Göttingen. EARZ was funded by an Emmy Noether Fellowship by Deutsche Forschungsgemeinschaft (#396913060).

DISCLOSURES
None.

SUPPLEMENTAL MATERIALS

Expanded Materials & Methods
Online Figures I – XII
Online Movies I – II
Data Set Excel Tables I – IV
Online Tables I – XIII
References 56–77

REFERENCES

1. Parton RG. Caveolae: structure, function, and relationship to disease. **Annu Rev Cell Dev Biol**. 2018; 34:111–136. DOI: 10.1146/annurev-cellbio-100617-062737
2. Sinha B, Köster D, Ruez R, Gonnord P, Bastiani M, Abankwa D, Stan RV, Butler-Browne G, Vedie B, Johannes L, Morone N, et al. Cells respond to mechanical stress by rapid disassembly of caveolae. **Cell**. 2011; 144:402–413. DOI: 10.1016/j.cell.2010.12.031
3. Ludwig A, Howard G, Mendoza-Topaz C, Deerinck T, Mackey M, Sandin S, Ellisman MH, Nichols BJ. Molecular composition and ultrastructure of the caveolar coat complex. **PLoS Biol**. 2013; 11:e1001640. DOI: 10.1371/journal.pbio.1001640
4. Morén B, Shah C, Howes MT, Schieber NL, McMahon HT, Parton RG, Daumke O, Lundmark R. EHD2 regulates caveolar dynamics via ATP-driven targeting and oligomerization. **Mol Biol Cell**. 2012; 23:1316–1329. DOI: 10.1091/mbc.E11-09-0787
5. Cohen AW, Park DS, Woodman SE, Williams TM, Chandra M, Shirani J, Pereira de Souza A, Kitsis RN, Russell RG, Weiss LM, et al. Caveolin-1 null mice develop cardiac hypertrophy with hyperactivation of p42/44 MAP kinase in cardiac fibroblasts. **Am J Physiol, Cell Physiol**. 2003; 284:C457-474. DOI: 10.1152/ajpcell.00380.2002
6. Robenek H, Weissen-Plenz G, Severs NJ. Freeze-fracture replica immunolabelling reveals caveolin-1 in the human cardiomyocyte plasma membrane. **J Cell Mol Med**. 2008; 12:2519–2521. DOI: 10.1111/j.1582-4934.2008.00498.x
7. Yang K-C, Rutledge CA, Mao M, Bakhshi FR, Xie A, Liu H, Bonini MG, Patel HH, Minshall RD, Dudley SC. Caveolin-1 modulates cardiac gap junction homeostasis and arrhythmogenecity by regulating cSrc tyrosine kinase. **Circ Arrhythm Electrophysiol**. 2014; 7:701–710. DOI: 10.1161/CIRCEP.113.001394
8. Ellinor PT, Lunetta KL, Albert CM, Glazer NL, Ritchie MD, Smith AV, Arking DE, Müller-Nurasyid M, Krijthe BP, Lubitz SA, et al. Meta-analysis identifies six new susceptibility loci for atrial fibrillation. **Nat Genet**. 2012; 44:670–675. doi: 10.1038/ng.2261
9. Vatta M, Ackerman MJ, Ye B, Makielski JC, Ughanze EE, Taylor EW, Tester DJ, Balijepalli RC, Foell JD, Li Z, et al. Mutant caveolin-3 induces persistent late sodium current and is associated with Long-QT syndrome. **Circulation**. 2006; 114:2104–2112. DOI: 10.1161/CIRCULATIONAHA.106.635268
10. Shvets E, Bitsikas V, Howard G, Hansen CG, Nichols BJ. Dynamic caveolae exclude bulk membrane proteins and are required for sorting of excess glycosphingolipids. **Nat Commun**. 2015; 6:6867. DOI: 10.1038/ncomms7867
11. Bosch M, Marí M, Herms A, Fernández A, Fajardo A, Kassan A, Giralt A, Colell A, Balgoma D, Barbero E, et al. Caveolin-1 deficiency causes cholesterol-dependent mitochondrial dysfunction and apoptotic susceptibility. **Curr Biol**. 2011; 21:681–686. DOI: 10.1016/j.cub.2011.03.030
12. Jóhannsson E, Lunde PK, Heddle C, Sjaastad I, Thomas MJ, Bergersen L, Halestrap AP, Blackstad TW, Ottersen OP, Sejersted OM. Upregulation of the cardiac monocarboxylate transporter MCT1 in a rat model of congestive heart failure. **Circulation**. 2001; 104:729–734. DOI: 10.1161/hc3201.092286

13. McNally EM, de Sá Moreira E, Duggan DJ, Bönnemann CG, Lisanti MP, Lidov HG, Vainzof M, Passos-Bueno MR, Hoffman EP, Zatz M, et al. Caveolin-3 in muscular dystrophy. **Hum Mol Genet**. 1998; 7:871–877. doi: 10.1093/hmg/7.5.871
14. Gavillet B, Rougier J-S, Domenighetti AA, Behar R, Boixel C, Ruchat P, Lehr H-A, Pedrazzini T, Abriel H. Cardiac sodium channel Nav1.5 is regulated by a multiprotein complex composed of syntrophins and dystrophin. **Circ Res**. 2006; 99:407–414. DOI: 10.1161/01.RES.0000237466.13252.5e
15. Lam SS, Martell JD, Kamer KJ, Deerinck TJ, Ellisman MH, Mootha VK, Ting AY. Directed evolution of APEX2 for electron microscopy and proximity labeling. **Nat Methods**. 2015; 12:51–54. DOI: 10.1038/nmeth.3179
16. Hung V, Zou P, Rhee H-W, Udeshi ND, Cracan V, Svinkina T, Carr SA, Mootha VK, Ting AY. Proteomic mapping of the human mitochondrial intermembrane space in live cells via ratiometric APEX tagging. **Mol Cell**. 2014; 55:332–341. DOI: 10.1016/j.molcel.2014.06.003
17. Kernik DC, Morotti S, Wu H, Garg P, Duff HJ, Kurokawa J, Jalife J, Wu JC, Grandi E, Clancy CE. A computational model of induced pluripotent stem-cell derived cardiomyocytes incorporating experimental variability from multiple data sources. **J Physiol**. 2019; 597:4533–4564. DOI: 10.1113/JP277724
18. Whiteley G, Collins RF, Kitmitto A. Characterization of the molecular architecture of human caveolin-3 and interaction with the skeletal muscle ryanodine receptor. **J Biol Chem**. 2012; 287:40302–40316. DOI: 10.1074/jbc.M112.377085
19. Ong S-E, Blagoev B, Kratchmarova I, Kristensen DB, Steen H, Pandey A, Mann M. Stable isotope labeling by amino acids in cell culture, SILAC, as a simple and accurate approach to expression proteomics. **Mol Cell Proteomics**. 2002; 1:376–386. DOI: 10.1074/mcp.m200025-mcp200
20. Szklarczyk D, Gable AL, Lyon D, Junge A, Wyder S, Huerta-Cepas J, Simonovic M, Doncheva NT, Morris JH, Bork P, et al. STRING v11: protein-protein association networks with increased coverage, supporting functional discovery in genome-wide experimental datasets. **Nucleic Acids Res**. 2019; 47:D607–D613. DOI: 10.1093/nar/gky1131
21. Parton RG, Collins BM. Unraveling the architecture of caveolae. **Proc Natl Acad Sci USA**. 2016; 113:14170–14172. doi: 10.1073/pnas.1617954113
22. Bastiani M, Parton RG. Caveolae at a glance. **J Cell Sci**. 2010; 123:3831–3836. DOI: 10.1242/jcs.070102
23. Hansen CG, Howard G, Nichols BJ. Pacsin 2 is recruited to caveolae and functions in caveolar biogenesis. **J Cell Sci**. 2011; 124:2777–2785. DOI: 10.1242/jcs.084319
24. Liu L, Askari A. Beta-subunit of cardiac Na+-K+-ATPase dictates the concentration of the functional enzyme in caveolae. **Am J Physiol, Cell Physiol**. 2006; 291:C569-578. DOI: 10.1152/ajpcell.00002.2006
25. Bossuyt J, Taylor BE, James-Kracke M, Hale CC. Evidence for cardiac sodium-calcium exchanger association with caveolin-3. **FEBS Lett**. 2002; 511:113–117. DOI: 10.1016/s0014-5793(01)03323-3
26. Volonte D, McTiernan CF, Drab M, Kasper M, Galbiati F. Caveolin-1 and caveolin-3 form heterooligomeric complexes in atrial cardiac myocytes that are required for doxorubicin-induced apoptosis. **Am J Physiol Heart Circ Physiol**. 2008; 294:H392–401. DOI: 10.1152/ajpheart.01039.2007
27. Schubert OT, Ludwig C, Kogadeeva M, Zimmermann M, Rosenberger G, Gengenbacher M, Gillet LC, Collins BC, Röst HL, Kaufmann SHE, et al. Absolute proteome composition and dynamics during dormancy and resuscitation of mycobacterium tuberculosis. **Cell Host Microbe**. 2015; 18:96–108. DOI: 10.1016/j.chom.2015.06.001
28. Tusher VG, Tibshirani R, Chu G. Significance analysis of microarrays applied to the ionizing radiation response. **Proc Natl Acad Sci USA**. 2001; 98:5116–5121. DOI: 10.1073/pnas.091062498
29. Birsoy K, Wang T, Possemato R, Yilmaz OH, Koch CE, Chen WW, Hutchins AW, Gultekin Y, Peterson TR, Carette JE, et al. MCT1-mediated transport of a toxic molecule is an effective strategy for targeting glycolytic tumors. **Nat Genet**. 2013; 45:104–108. DOI: 10.1038/ng.2471

30. Sprowl-Tanio S, Habowski AN, Pate KT, McQuade MM, Wang K, Edwards RA, Grun F, Lyou Y, Waterman ML. Lactate/pyruvate transporter MCT-1 is a direct Wnt target that confers sensitivity to 3-bromopyruvate in colon cancer. **Cancer Metab**. 2016; 4:20. DOI: 10.1186/s40170-016-0159-3
31. Ehrke E, Arend C, Dringen R. 3-bromopyruvate inhibits glycolysis, depletes cellular glutathione, and compromises the viability of cultured primary rat astrocytes. **J Neurosci Res**. 2015; 93:1138–1146. DOI: 10.1002/jnr.23474
32. Garcia CK, Goldstein JL, Pathak RK, Anderson RG, Brown MS. Molecular characterization of a membrane transporter for lactate, pyruvate, and other monocarboxylates: implications for the Cori cycle. **Cell**. 1994; 76:865–873. DOI: 10.1016/0092-8674(94)90361-1
33. Rose S, Frye RE, Slattery J, Wynne R, Tippett M, Pavliv O, Melnyk S, James SJ. Oxidative stress induces mitochondrial dysfunction in a subset of autism lymphoblastoid cell lines in a well-matched case control cohort. **PLoS ONE**. 2014; 9:e85436. DOI: 10.1371/journal.pone.0085436
34. Wang X, Cai L, Xie JX, Cui X, Zhang J, Wang J, Chen Y, Larre I, Shapiro JI, Pierre SV, et al. A caveolin binding motif in Na/K-ATPase is required for stem cell differentiation and organogenesis in mammals and C.elegans. **Sci Adv**. 2020; 6:eaaw5851. DOI: 10.1126/sciadv.aaw5851
35. Balijepalli RC, Kamp TJ. Caveolae, ion channels and cardiac arrhythmias. **Prog Biophys Mol Biol**. 2008; 98:149–160. DOI: 10.1016/j.pbiomolbio.2009.01.012
36. Vaidyanathan R, Reilly L, Eckhardt LL. Caveolin-3 microdomain: arrhythmia implications for potassium inward rectifier and cardiac sodium channel. **Front Physiol**. 2018; 9:1548. DOI: 10.3389/fphys.2018.01548
37. Yarbrough TL, Lu T, Lee H-C, Shibata EF. Localization of cardiac sodium channels in caveolin-rich membrane domains: regulation of sodium current amplitude. **Circ Res**. 2002; 90:443–449. DOI: 10.1161/hh0402.105177
38. Wan E, Abrams J, Weinberg RL, Katchman AN, Bayne J, Zakharov SI, Yang L, Morrow JP, Garan H, Marx SO. Aberrant sodium influx causes cardiomyopathy and atrial fibrillation in mice. **J Clin Invest**. 2016; 126:112–122. DOI: 10.1172/JCI84669
39. Milstein ML, Musa H, Balbuena DP, Anumonwo JMB, Auerbach DS, Furspan PB, Hou L, Hu B, Schumacher SM, Vaidyanathan R, et al Dynamic reciprocity of sodium and potassium channel expression in a macromolecular complex controls cardiac excitability and arrhythmia. **Proc Natl Acad Sci USA**. 2012; 109:E2134-2143. doi: 10.1073/pnas.1109370109
40. Alsina KM, Hulsurkar M, Brandenburg S, Kownatzki-Danger D, Lenz C, Urlaub H, Abu-Taha I, Kamler M, Chiang DY, Lahiri SK, et al. Loss of protein phosphatase 1 regulatory subunit PPP1R3A promotes atrial fibrillation. **Circulation**. 2019; 140:681–693. DOI: 10.1161/CIRCULATIONAHA.119.039642
41. Jóhannsson E, Nagelhus EA, McCullagh KJ, Sejersted OM, Blackstad TW, Bonen A, Ottersen OP. Cellular and subcellular expression of the monocarboxylate transporter MCT1 in rat heart. A high-resolution immunogold analysis. **Circ Res**. 1997; 80:400–407. PMID: 9048661
42. van der Vusse GJ, de Groot MJ. Interrelationship between lactate and cardiac fatty acid metabolism. *Mol Cell Biochem*. 1992; 116:11–17. DOI: 10.1007/BF01270563
43. Vandenberg JI, Metcalfe JC, Grace AA. Mechanisms of pHi recovery after global ischemia in the perfused heart. **Circ Res**. 1993; 72:993–1003. DOI: 10.1161/01.res.72.5.993
44. Rana P, Anson B, Engle S, Will Y. Characterization of human-induced pluripotent stem cell–derived cardiomyocytes: bioenergetics and utilization in safety screening. **Toxicol Sci**. 2012; 130:117–131. DOI: 10.1093/toxsci/kfs233
45. Doherty JR, Yang C, Scott KEN, Cameron MD, Fallahi M, Li W, Hall MA, Amelio AL, Mishra JK, Li F, et al. Blocking lactate export by inhibiting the Myc target MCT1 disables glycolysis and glutathione synthesis. **Cancer Res**. 2014; 74:908–920. DOI: 10.1158/0008-5472.CAN-13-2034
46. Deng YF, Huang YY, Lu WS, Huang YH, Xian J, Wei HQ, Huang Q. The Caveolin-3 P104L mutation of LGMD-1C leads to disordered glucose metabolism in muscle cells. **Biochem Biophys Res Commun**. 2017; 486:218–223. DOI: 10.1016/j.bbrc.2017.02.072

47. Dewulf M, Köster DV, Sinha B, Lesegno CV de, Chambon V, Bigot A, Bensalah M, Negroni E, Tardif N, Podkalicka J, et al. Dystrophy-associated caveolin-3 mutations reveal that caveolae couple IL6/STAT3 signaling with mechanosensing in human muscle cells. **Nat Commun**. 2019; 10:1–13. DOI: 10.1038/s41467-019-09405-5
48. Jóhannsson E, Nagelhus EA, McCullagh KJ, Sejersted OM, Blackstad TW, Bonen A, Ottersen OP. Cellular and subcellular expression of the monocarboxylate transporter MCT1 in rat heart. A high-resolution immunogold analysis. **Circ Res**. 1997; 80:400–407. PMID: 9048661
49. Wyse BD, Prior IA, Qian H, Morrow IC, Nixon S, Muncke C, Kurzchalia TV, Thomas WG, Parton RG, Hancock JF. Caveolin interacts with the angiotensin II type 1 receptor during exocytic transport but not at the plasma membrane. **J Biol Chem**. 2003; 278:23738–23746. DOI: 10.1074/jbc.M212892200
50. Horikawa YT, Panneerselvam M, Kawaraguchi Y, Tsutsumi YM, Ali SS, Balijepalli RC, Murray F, Head BP, Niesman IR, Rieg T, et al. Cardiac-specific overexpression of caveolin-3 attenuates cardiac hypertrophy and increases natriuretic peptide expression and signaling. **J Am Coll Cardiol**. 2011; 57:2273–2283. DOI: 10.1016/j.jacc.2010.12.032
51. Han B, Copeland CA, Tiwari A, Kenworthy AK. Assembly and turnover of caveolae: what do we really know? ***Front Cell Dev Biol***. 2016; 4. DOI: 10.3389/fcell.2016.00068
52. Cao H, Courchesne WE, Mastick CC. A Phosphotyrosine-dependent protein interaction screen reveals a role for phosphorylation of caveolin-1 on tyrosine 14 recruitment of C-terminal Src kinase. **J Biol Chem**. 2002; 277:8771–8774. DOI: 10.1074/jbc.C100661200
53. Parton RG, del Pozo MA. Caveolae as plasma membrane sensors, protectors and organizers. **Nat Rev Mol Cell Biol**. 2013; 14:98–112. DOI: 10.1038/nrm3512
54. Hayer A, Stoeber M, Ritz D, Engel S, Meyer HH, Helenius A. Caveolin-1 is ubiquitinated and targeted to intralumenal vesicles in endolysosomes for degradation. **J Cell Biol**. 2010; 191:615–629. DOI: 10.1083/jcb.201003086
55. Aravamudan B, Volonte D, Ramani R, Gursoy E, Lisanti MP, London B, Galbiati F. Transgenic overexpression of caveolin-3 in the heart induces a cardiomyopathic phenotype. **Hum Mol Genet**. 2003; 12:2777–2788. DOI: 10.1093/hmg/ddg313
56. Razani B, Engelman JA, Wang XB, Schubert W, Zhang XL, Marks CB, Macaluso F, Russell RG, Li M, Pestell RG, et al. Caveolin-1 null mice are viable but show evidence of hyperproliferative and vascular abnormalities. **J Biol Chem**. 2001; 276:38121–38138. DOI: 10.1074/jbc.M105408200
57. Rutering J, Ilmer M, Recio A, Coleman M, Vykoukal J, Alt E. Improved method for isolation of neonatal rat cardiomyocytes with increased yield of C-Kit+ cardiac progenitor cells. **J Stem Cell Res Ther**. 2015; 5:1–8. DOI: 10.4172/2157-7633.1000305
58. Atanassov I, Urlaub H. Increased proteome coverage by combining PAGE and peptide isoelectric focusing: Comparative study of gel-based separation approaches. **Proteomics**. 2013; 13:2947–2955. DOI: 10.1002/pmic.201300035
59. Perez-Riverol Y, Csordas A, Bai J, Bernal-Llinares M, Hewapathirana S, Kundu DJ, Inuganti A, Griss J, Mayer G, Eisenacher M, et al. The PRIDE database and related tools and resources in 2019: improving support for quantification data. **Nucleic Acids Res**. 2019; 47:D442–D450. DOI: 10.1093/nar/gky1106
69. Lambert J-P, Ivosev G, Couzens AL, Larsen B, Taipale M, Lin Z-Y, Zhong Q, Lindquist S, Vidal M, Aebersold R ,et al. Mapping differential interactomes by affinity purification coupled with data-independent mass spectrometry acquisition. **Nat Methods**. 2013; 10:1239–1245. DOI: 10.1038/nmeth.2702
61. Zhang Y, Bilbao A, Bruderer T, Luban J, Strambio-De-Castillia C, Lisacek F, Hopfgartner G, Varesio E. The use of variable Q1 isolation windows improves selectivity in LC-SWATH-MS acquisition. **J Proteome Res**. 2015; 14:4359–4371. DOI: 10.1021/acs.jproteome.5b00543
62. Erdmann J, Thöming JG, Pohl S, Pich A, Lenz C, Häussler S. The core proteome of biofilm-grown clinical pseudomonas aeruginosa isolates. **Cells**. 2019; 8:1129. DOI: 10.3390/cells8101129

63. Oliveira GS, Santos AR. Using the gene ontology tool to produce de novo protein-protein interaction networks with IS_A relationship. **Genet Mol Res**. 2016; 15(4). DOI: 10.4238/gmr15049273
64. Cyganek L, Tiburcy M, Sekeres K, Gerstenberg K, Bohnenberger H, Lenz C, Henze S, Stauske M, Salinas G, Zimmermann W-H, et al. Deep phenotyping of human induced pluripotent stem cell–derived atrial and ventricular cardiomyocytes. **JCI Insight**. 2018; 3:e99941. DOI: 10.1172/jci.insight.99941
65. Zhao L, Hayes K, Glassman A. A simple efficient method of sequential G-banding and fluorescence in situ hybridization. **Cancer Genet Cytogenet**. 1998; 103:62–64. DOI: 10.1016/s0165-4608(97)00345-2
66. O'Connell TD, Rodrigo MC, Simpson PC. Isolation and culture of adult mouse cardiac myocytes. **Methods Mol Biol**. 2007; 357:271–296. DOI: 10.1385/1-59745-214-9:271
67. Wagner E, Brandenburg S, Kohl T, Lehnart SE. Analysis of tubular membrane networks in cardiac myocytes from atria and ventricles. **J Vis Exp**. 2014; 92:e51823. DOI: 10.3791/51823
68. Poulet C, Wettwer E, Grunnet M, Jespersen T, Fabritz L, Matschke K, Knaut M, Ravens U. Late sodium current in human atrial cardiomyocytes from patients in sinus rhythm and atrial fibrillation. **PLOS ONE**. 2015; 10:e0131432. DOI: 10.1371/journal.pone.0131432
69. Wettwer E, Christ T, Endig S, Rozmaritsa N, Matschke K, Lynch JJ, Pourrier M, Gibson JK, Fedida D, Knaut M, Ravens U. The new antiarrhythmic drug vernakalant: ex vivo study of human atrial tissue from sinus rhythm and chronic atrial fibrillation. **Cardiovasc Res**. 2013; 98:145–154. DOI: 10.1093/cvr/cvt006
70. Sossalla S, Kallmeyer B, Wagner S, Mazur M, Maurer U, Toischer K, Schmitto JD, Seipelt R, Schöndube FA, Hasenfuss G, et al. Altered Na(+) currents in atrial fibrillation effects of ranolazine on arrhythmias and contractility in human atrial myocardium. **J Am Coll Cardiol**. 2010; 55:2330–2342. DOI: 10.1016/j.jacc.2009.12.055
71. Berry R, Despa S, Fuller W, Bers D, Shattock M. Differential distribution and regulation of mouse cardiac Na+/K+-ATPase alpha1 and alpha2 subunits in T-tubule and surface sarcolemmal membranes. **Cardiovasc Res**. 2006; 73:92–100. DOI: 10.1016/j.cardiores.2006.11.006
72. Fine M, Lu F-M, Lin M-J, Moe O, Wang H-R, Hilgemann DW. Human-induced pluripotent stem cell-derived cardiomyocytes for studies of cardiac ion transporters. **Am J Physiol Cell Physiol**. 2013; 305:C481-491. DOI: 10.1152/ajpcell.00143.2013
73. Clerx M, Collins P, de Lange E, Volders PGA. Myokit: a simple interface to cardiac cellular electrophysiology. **Prog Biophys Mol Biol**. 2016; 120:100–114. DOI: 10.1016/j.pbiomolbio.2015.12.008
74. Brandenburg S, Pawlowitz J, Fakuade FE, Kownatzki-Danger D, Kohl T, Mitronova GY, Scardigli M, Neef J, Schmidt C, Wiedmann F, et al. Axial tubule junctions activate atrial Ca2+ release across species. **Front Physiol**. 2018; 9:1227. DOI: 10.3389/fphys.2018.01227
75. Mastronarde DN. Dual-axis tomography: an approach with alignment methods that preserve resolution. **J Struct Biol**. 1997; 120:343–352. DOI: 10.1006/jsbi.1997.3919
76. Mastronarde DN, Held SR. Automated tilt series alignment and tomographic reconstruction in IMOD. **J Struct Biol**. 2017; 197:102–113. doi: 10.1016/j.jsb.2016.07.011.
77. Kremer JR, Mastronarde DN, McIntosh JR. Computer visualization of three-dimensional image data using IMOD. **J Struct Biol**. 1996; 116:71–76. DOI: 10.1006/jsbi.1996.0013

FIGURE LEGENDS

Figure 1. Targeting the CAV3 complex for proximity proteomics. A, CAV3 was N-terminally tagged by V5 and APEX2 for expression in neonatal rat cardiomyocytes (NRCM). Upon treatment of NRCMs with peroxide (1 mmol/L H_2O_2 for 1 min) APEX2 generates a reactive cloud of biotinphenoxyl radical (red) that covalently labels proteins-of-interest (POI) in nanometric proximity. B, biotinphenol; IC, intracellular. **B,** Representative immunoblot comparing V5-APEX2-CAV3 expressed by plasmid versus adenoviral transfection in NRCMs. Bar graph summarizing V5-APEX2-CAV3 expression normalized to endogenous CAV3. n=3, *** $p<0.001$, unpaired two-tailed t-test, Prism version 7.03. **C,** V5 co-immunoprecipitation (IP) followed by immunoblotting confirmed that V5-APEX2-CAV3 binds to endogenous CAV3 (✶) but not the soluble V5-APEX2 control in NRCMs. n=3. **D,** Blue native (BN) gradient gel separation and immunoblotting of V5-APEX2-CAV3 in NRCMs. A major high MW complex ≥545 kDa was detected by CAV3 immunoblotting in untransfected (control) and V5-APEX2-CAV3 transfected NRCMs. V5 immunoblotting confirmed V5-APEX2-CAV3 in the high molecular weight complex in adenovirally transfected but not in untransfected NRCMs (control). n=3. **E**, Confocal imaging of adenovirally transfected NRCMs (MOI 1) showing co-localized V5-APEX2-CAV3 with endogenous CAV3. Scale bars, each image 10 μm.

Figure 2. Ratiometric proximity proteomics identifies new CAV3 interactor candidates. A, Systematic workflow for quantitative NRCM protein labeling by 3-state SILAC switching in 35 mm culture dishes. NRCMs were labeled with light (L), medium (M), or heavy (H) L-arginine and L-lysine isotopes as indicated, followed by adenoviral transfection of V5-APEX2-CAV3 versus V5-APEX2 (control-1) or eGFP (control-2). **B**, LC-MS/MS analysis showed >96.5% L-arginine (Arg) and L-lysine (Lys) incorporation (red dashed line 95%). n=3. **C**, APEX2 biotinylated proteins were captured by avidin. I, input; FT, flow through; E, eluate. V5-APEX2-CAV3 and V5-APEX2 expression confirmed by V5 immunoblotting. n=3. **D**, Scatter plot showing the indicated logarithmic ratios of enriched proteins identified by LC-MS/MS. Positive hits are represented by blue and yellow color ($p<0.05$; z-test), the latter highlighting functionally relevant hits further analyzed by GO analysis. n=3. **E**, Exploration of CAV3 interactions based on the STRING database for the GO terms 'caveolae', 'muscle contraction', 'pyruvate metabolism', and 'iron uptake'. Coloring analogous to panel **D**. Protein-protein interactions are represented by grey lines based on a confidence score ≥0.7.

Figure 3. CAV1 is differentially distributed in ventricular cardiomyocytes. A, Immunoblotting showed a specific CAV1 signal in ventricular cardiomyocytes of WT hearts, but not in CAV1 knockout mouse hearts. n=3. **B**, DIA-MS was used to determine the relative concentrations of three caveolin isoforms. The CAV1 protein area was significantly larger compared to CAV2 or CAV3. n=5. *** $p<0.001$, two-way ANOVA, Prism version 7.03. **C**, Ranking of all proteins detected by DIA-MS protein area positions CAV1 among the most abundant proteins. n=5. **D**, Confocal and STED co-immunofluorescence imaging of CAV1 and CAV3 clusters in ventricular cardiomyocytes. Dashed boxes indicate magnified regions of interest at the intercalated disk and transverse tubules, where STED superresolution nanoscopy resolved differential CAV1 versus CAV3 cluster signal distributions. Scale bars, top image 10 μm; confocal and STED image panels each 2 μm; STED magnifications each 200 nm. **E**, Reciprocal co-immunoprecipitation of CAV1 versus CAV3. Immunoblotting showed strong homomeric versus weak heteromeric interactions between native CAV1 and/or CAV3. Negative control, rabbit IgG. n=3.

Figure 4. Identification of differential protein interactions by AP-MS. **A**, Volcano plot comparing CAV1 and CAV3 interacting proteins identified by AP-MS. Logarithmic ratios identify enriched CAV1 and CAV3 interacting proteins indicated as positive hits (blue circles) including functionally relevant proteins of interest (yellow circles). Positive hits and proteins of interest were identified by permutation-based false discovery rate analysis (t-test, $p>0.05$, FDR=5%, S0=0.1, Perseus version 1.5.6.0) and logarithmic cut-off

≥1 (dashed line). Negative hits were excluded based on the same criteria. n=3. **B**, Bar graph comparing the logarithmic ratio (control IgG) of candidate protein interactions between CAV1 and/or CAV3. A log(2) fold-change >1 was used as cut-off (dashed lanes). * p<0.001, unpaired two-tailed t-test, Prism version 7.03. **C**, Immunoprecipitation followed by immunoblotting was used to confirm candidate protein interactions. Rabbit IgG served as negative control. n=3. **D**, Confocal and STED co-immunofluorescence imaging of CAV3 and McT1 in ventricular myocytes. *Left*: cartoon of a ventricular cardiomyocyte documenting the subcellular imaging planes used for confocal and STED imaging. Dashed boxes indicate regions of representative high-power magnifications. Scale bars, confocal and STED image panels each 1 µm; magnifications each 200 nm.

Figure 5. CAV3 KO disrupts McT1 function in human cardiomyocytes. A, Immunoblot analysis of human iPSC-derived CAV3 knockout (KO) cardiomyocytes. CAV3 and McT1 were robustly expressed, while CAV3 signal specificity was confirmed in CAV3 KO cardiomyocytes. Bar graph showing significant reduction of global McT1 expression in CAV3 KO cardiomyocytes normalized to β-Actin. n=3. Unpaired two-tailed t-test, Prism version 7.03., * p<0.05. **B**, Extracellular protein biotinylation in living human cardiomyocytes assessing McT1 surface expression. Biotinylated proteins were enriched by pull-down and McT1 identified by immunoblotting in the eluted fraction. Vice versa, β-Actin immunoblotting was used as negative control. Bar graph showing a significant loss of surface McT1 in CAV3 KO versus WT cardiomyocytes. n=3. Unpaired two-tailed t-test, Prism version 7.03., * p<0.05. **C**, Following uptake of 3-bromopyruvate (3-BrPA), a glycolysis-disrupting compound, cell viability was assessed by extracellular release of lactate dehydrogenase (LDH). Bar graph confirming a significantly reduced LDH release from CAV3 KO cardiomyocytes incubated with 50 µmol/L 3-BrPA. n=6. Unpaired two-tailed t-test, Prism version 7.03., *** p<0.001. **D**, The oxygen consumption rate (OCR) of human cardiomyocytes was not affected by CAV3 KO. n=32. Unpaired two-tailed t-test, Prism version 7.03. **E**, The extracellular acidification rate (ECAR) was blunted by CAV3 KO at baseline and after oligomycin treatment. n=32. Unpaired two-tailed t-test, Prism version 7.03., * p<0.05; **p<0.01; *** p<0.001.

Figure 6. CAV3 knockout (KO) causes prolonged action potential duration (APD), early afterdepolarizations (EADs), and increased late Na^+ currents ($I_{Na,L}$) in human iPSC-derived cardiomyocytes (iPSC-CMs). **A**, Action potential traces from WT versus CAV3 KO iPSC-CMs. **B**, Dot plot summarizing APD_{50} and APD_{90} values from individual iPSC-CM voltage-imaging experiments. WT, n=8; CAV3 KO, n=17. Unpaired two-tailed t-test, Prism version 7.03. *p<0.05, ***p<0.001. **C**, Dot plot comparing the repolarization fraction of WT versus CAV3 KO iPSC-CMs. WT, n=8; CAV3 KO, n=17. Unpaired two-tailed t-test, Prism version 7.03. ***p<0.001. **D**, Action potential event traces of WT versus CAV3 KO iPSC-CMs. Triangles indicate early afterdepolarization (EAD) events. **E**, Classification (%) of voltage traces without versus traces with EAD events between human WT versus CAV3 KO iPSC-CMs. Cell numbers per group without versus with EAD events are indicated. **F**, *left*: representative peak Na^+ current (I_{Na}) traces and voltage protocol (inset); *right*: current density-voltage (IV) relations for WT (n=10) and CAV3 KO (n=16) iPSC-CMs. **G**, *left*: representative late Na^+ current ($I_{Na,L}$) WT and KO iPSC-CM traces, before and after $I_{Na,L}$ inhibition by 10 µmol/L TTX; *right*: dot plot representing $I_{Na,L}$ within 50 to 250 ms after the depolarizing pulse at -30 mV. WT n=10; KO n=16. Unpaired two-tailed t-test, Prism version 8.4.2. *p<0.05, **p<0.01. **H**, Simulated spontaneous action potentials in the original (EAD-resistant) iPSC-CM model (*left*) versus the EAD-prone cell model with a reduced repolarization reserve (*right*), comparing WT (*top*) versus increased $I_{Na,L}$ (*bottom*) conditions. Model details are provided in the Data Supplement. **I**, *left*: Two-dimensional cardiac tissue simulation representing both WT-like (1) and central EAD-prone (2) regions; *right*: a figure-of-eight reentry lasting >9 seconds is elicited in response to a single pacing stimulus from the left side of the tissue (arrow). The complete movie of the simulation is available (Video II in the Data Supplement) and sequential snapshots of the reentry are provided (Figure X in the Data Supplement).

Figure 7. CAV3 does not co-immunoprecipitate or co-localize with $Na_V1.5$ in adult mouse cardiomyocytes. **A**, Transgenic human FLAG-$Na_V1.5$ or WT mouse heart $Na_V1.5$ (control) were immunoprecipitated using the protocol of Vatta et al[9]. Input: immunoblotting identified both the native mouse $Na_V1.5$, the human FLAG-$Na_V1.5$, and abundant CAV3. IP FLAG: immunoblotting detecting both FLAG and $Na_V1.5$ of the human protein, but not mouse $Na_V1.5$. However, CAV3 was not detected. n=4 independent experiments. **B**, Using the protocol of Milstein et al[39], immunoblotting identified both native $Na_V1.5$ and SAP97 (positive control) in WT mouse heart lysates after immunoprecipitation, however, CAV3 was not detected. n=2 independent experiments. **C**, Confocal and STED imaging of WT mouse cardiomyocytes immunostained for CAV3 and $Na_V1.5$. While confocal imaging suggested co-localized CAV3 signals at T-tubule striations, STED nanoscopy excluded co-localized, but resolved spatially segregated CAV3 and $Na_V1.5$ cluster signals frequently near each other (magnification). Dashed boxes (top and middle panels) indicate magnified regions. Scale bars, top images each 10 μm; middle images each 1 μm; magnifications each 200 nm. Green triangles mark the position of one exemplary T-tubule striation labeled by CAV3 immunostaining. n=2 independent experiments.

Figure 8. Complexome profiling after live-cell cross-linking identifies CAV3 multimers in labile protein assemblies with multiple transmembrane transporter complexes in mouse cardiomyocytes. Untreated versus DSS treated living adult mouse ventricular cardiomyocytes were lysed, protein complexes separated by BN-PAGE and 23 gel fractions analyzed individually by MS. **A** and **C**, Abundance heat maps representing membrane protein complexes according to normalized signal intensity and calibrated apparent molecular mass as indicated. **B** and **D**, Corresponding protein abundance line profiles of CAV3, McT1, the Na,K-ATPase α1 subunit, and Ncx1. **B**, The peak abundance of the CAV3 complex at ~300 kDa (cyan) is clearly segregated from each the McT1, Na,K-ATPase α1, and Ncx1 peaks under untreated conditions. **D**, Live-cell cross-linking (DSS 0.1 mmol/L) resulted in a leftward shift and additional minor peaks in the 100-400 kDa range each for McT1, Na,K-ATPase α1, and Ncx1, partly overlapping the major CAV3 peak (arrow). n=3 cardiomyocyte isolations from 3 WT mice.

NOVELTY AND SIGNIFICANCE

What Is Known?

- Caveolin3 gene variants can cause a spectrum of striated muscle diseases including cardiac arrhythmias and a cardiomyopathy classified as Long-QT syndrome type 9.
- Previously, Western blotting showed that Caveolin1 is expressed in adult left-ventricular mouse cardiomyocytes.
- To date, differential isoform-specific Caveolin functions through heterologous protein interactions remain unexplored in muscle cells.

What New Information Does This Article Contribute?

- Quantitative mass spectrometry profiling revealed that Caveolin1 is highly abundant and thus ubiquitously expressed, whereas the muscle-specific Caveolin3 isoform is far less abundant in ventricular mouse cardiomyocytes.
- The main cardiac and metabolically relevant transmembrane lactate/proton shuttle, the monocarboxylate transporter McT1, was identified as a novel isoform-specific Caveolin3 interactor.
- CRISPR/Cas9-targeted CAV3 knock-out in human iPSC-derived cardiomyocytes disrupts functional McT1 surface expression in the sarcolemmal membrane. CAV3 knock-out increased late transmembrane Na^+ currents 2-fold leading to arrhythmogenic early afterdepolarizations and reentry arrhythmias in a corresponding multicellular mathematical tissue model.

The findings demonstrate that Caveolin3 loss-of-function causes multifactorial defects in cardiomyocytes including action potential instability and disrupted lactate/proton co-transport, which is important for cardiac stress adaptation. Identification of isoform-specific heterologous Caveolin1 and Caveolin3 protein interactions in cardiomyocytes provides a conceptual framework, which facilitates the systematic exploration of previously unknown interactomic functions throughout cardiac, skeletal, and smooth muscle cell types. Rare pathogenic Caveolin1 and Caveolin3 gene variants, as well as Caveolin1 single nucleotide polymorphisms associated with common arrhythmogenic cardiac phenotypes previously, require future study in the context of cardiac and skeletal muscle dysfunction in patients.

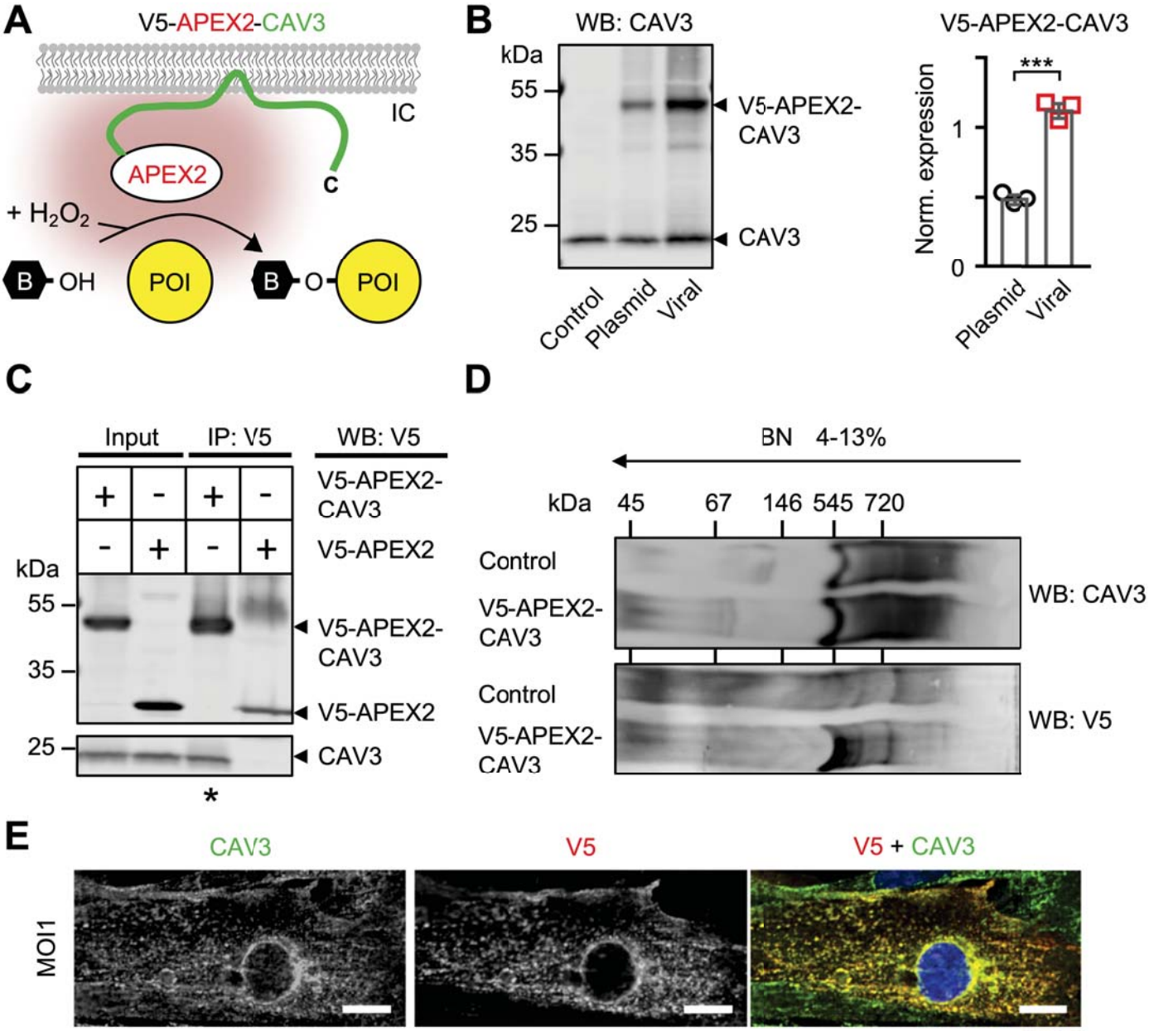
A
V5-APEX2-CAV3
IC
APEX2
C
+ H2O2
B
OH
POI
B
O
POI
B
WB: CAV3
kDa
55
35
25
V5-APEX2-CAV3
CAV3
Control
Plasmid
Viral
V5-APEX2-CAV3
***
Norm. expression
1
0
Plasmid
Viral
C
Input
IP: V5
WB: V5
+
-
+
-
V5-APEX2-CAV3
-
+
-
+
V5-APEX2
kDa
55
35
25
V5-APEX2-CAV3
V5-APEX2
CAV3
*
D
BN 4-13%
kDa
45
67
146
545
720
Control
V5-APEX2-CAV3
WB: CAV3
Control
V5-APEX2-CAV3
WB: V5
E
CAV3
V5
V5 + CAV3
MOI1

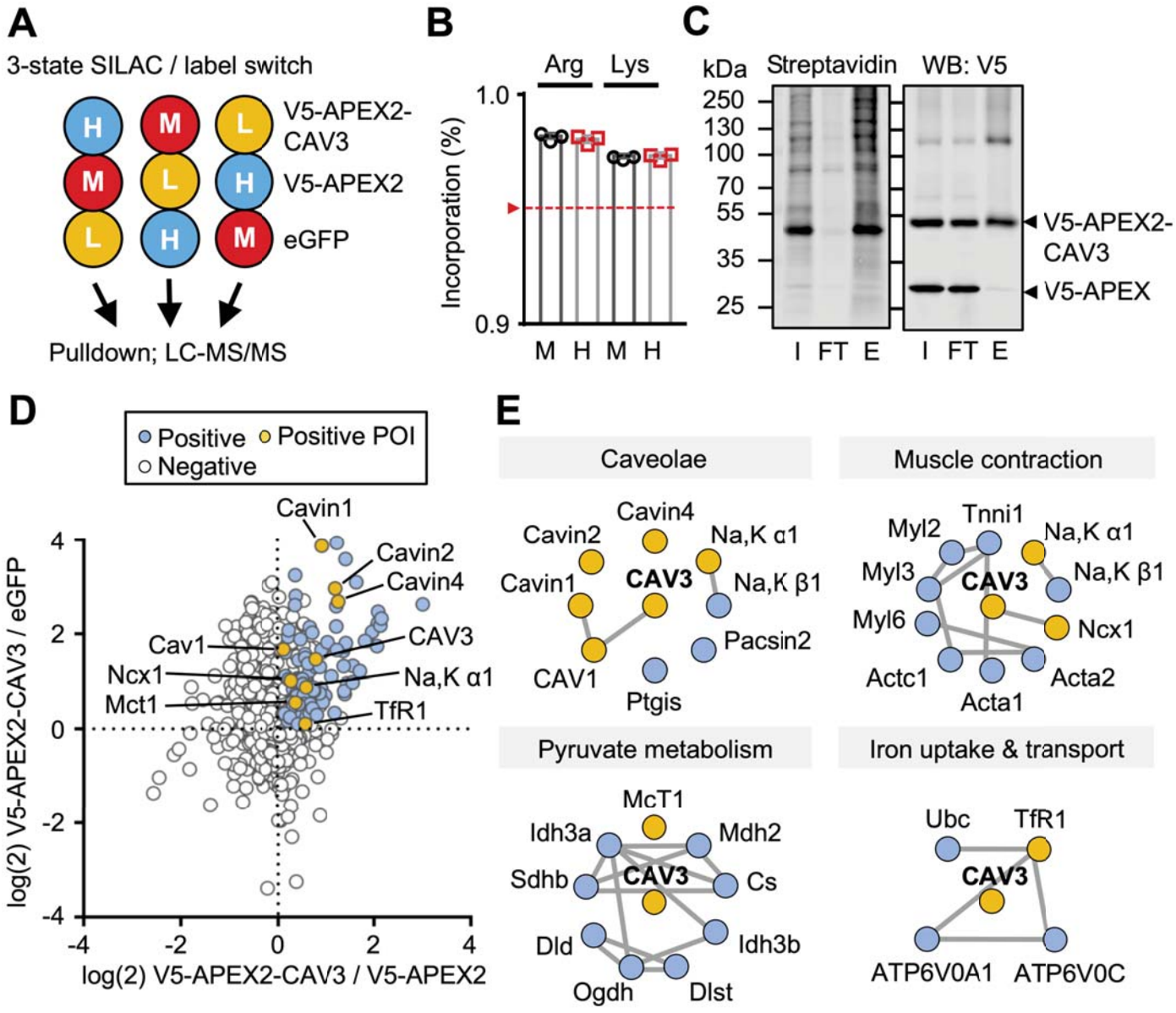
A
3-state SILAC / label switch
V5-APEX2-CAV3
V5-APEX2
eGFP
Pulldown; LC-MS/MS
B
Arg
Lys
Incorporation (%)
1.0
0.9
M H M H
C
kDa
Streptavidin
WB: V5
250
130
100
70
55
35
25
V5-APEX2-CAV3
V5-APEX
I FT E I FT E
D
Positive
Positive POI
Negative
log(2) V5-APEX2-CAV3 / eGFP
log(2) V5-APEX2-CAV3 / V5-APEX2
Cavin1
Cavin2
Cavin4
CAV3
Cav1
Ncx1
Mct1
Na,K α1
TfR1
E
Caveolae
Cavin4
Cavin2
Na,K α1
Cavin1
CAV3
Na,K β1
Pacsin2
CAV1
Ptgis
Muscle contraction
Tnni1
Myl2
Na,K α1
Myl3
CAV3
Na,K β1
Myl6
Ncx1
Actc1
Acta2
Acta1
Pyruvate metabolism
McT1
Idh3a
Mdh2
Sdhb
CAV3
Cs
Dld
Idh3b
Ogdh
Dlst
Iron uptake & transport
Ubc
TfR1
CAV3
ATP6V0A1
ATP6V0C

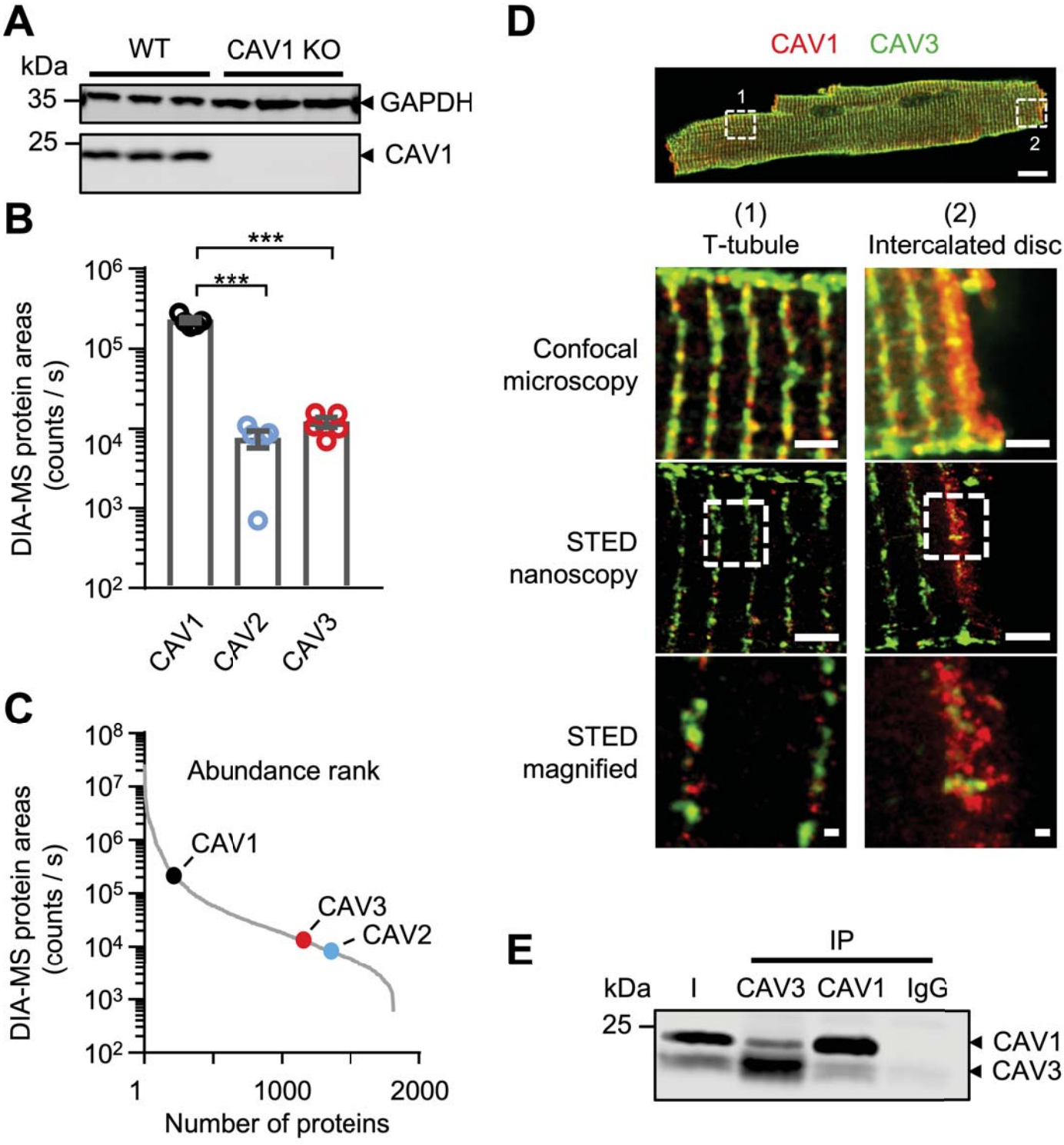
A
WT
CAV1 KO
kDa
35
GAPDH
25
CAV1
B
***
***
DIA-MS protein areas (counts / s)
10^6
10^5
10^4
10^3
10^2
CAV1
CAV2
CAV3
C
Abundance rank
DIA-MS protein areas (counts / s)
10^8
10^7
10^6
10^5
10^4
10^3
10^2
CAV1
CAV3
CAV2
1
1000
2000
Number of proteins
D
CAV1
CAV3
1
2
(1)
T-tubule
(2)
Intercalated disc
Confocal microscopy
STED nanoscopy
STED magnified
E
IP
kDa
I
CAV3
CAV1
IgG
25
CAV1
CAV3

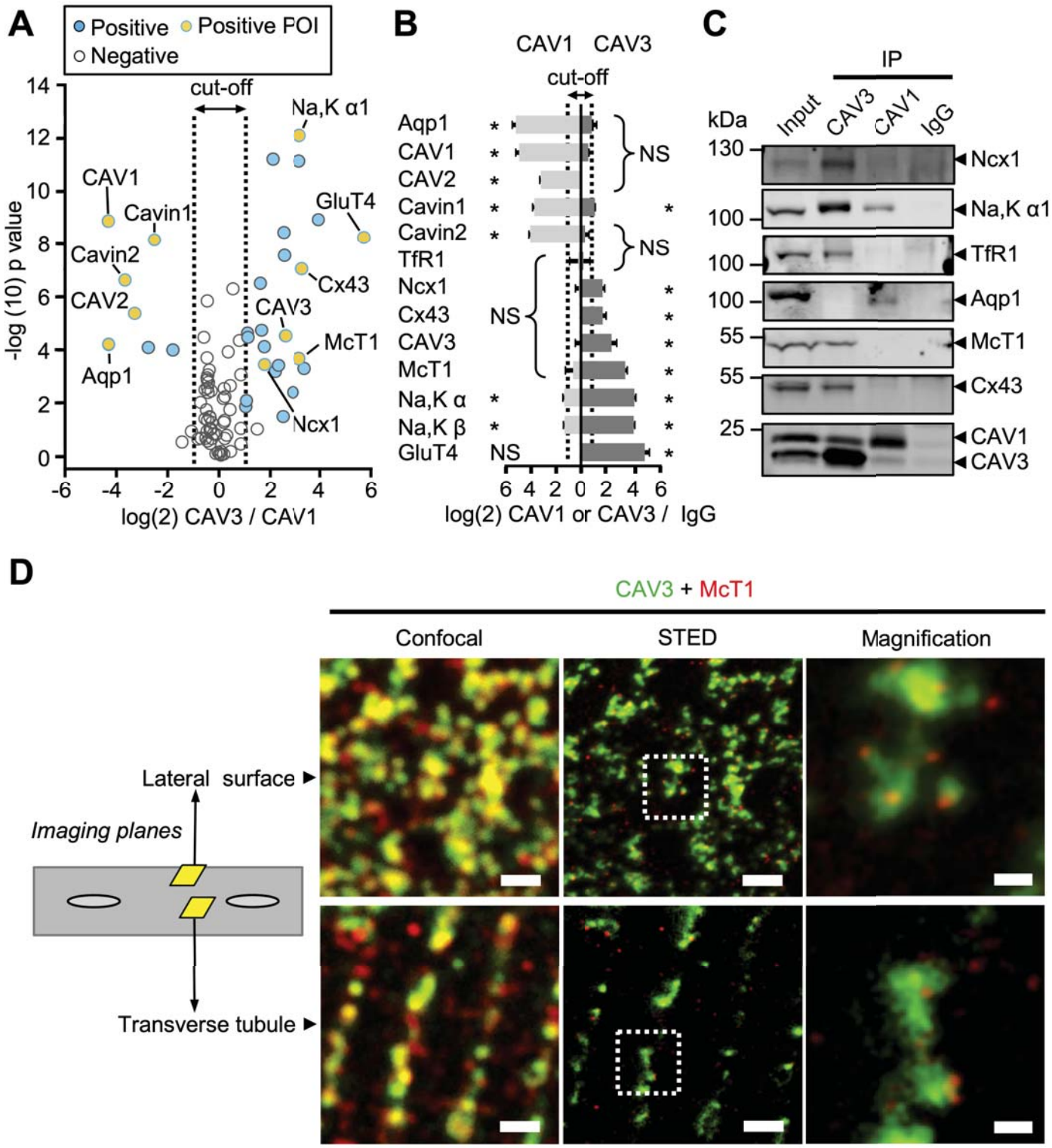
A
Positive
Positive POI
Negative
cut-off
-log (10) p value
log(2) CAV3 / CAV1
Na,K α1
CAV1
Cavin1
GluT4
Cavin2
Cx43
CAV2
CAV3
McT1
Aqp1
Ncx1
B
CAV1
CAV3
cut-off
Aqp1
CAV1
CAV2
Cavin1
Cavin2
TfR1
Ncx1
Cx43
CAV3
McT1
Na,K α
Na,K β
GluT4
NS
log(2) CAV1 or CAV3 / IgG
C
IP
kDa
Input
CAV3
CAV1
IgG
130
100
100
100
55
55
25
Ncx1
Na,K α1
TfR1
Aqp1
McT1
Cx43
CAV1
CAV3
D
CAV3 + McT1
Confocal
STED
Magnification
Lateral surface
Imaging planes
Transverse tubule

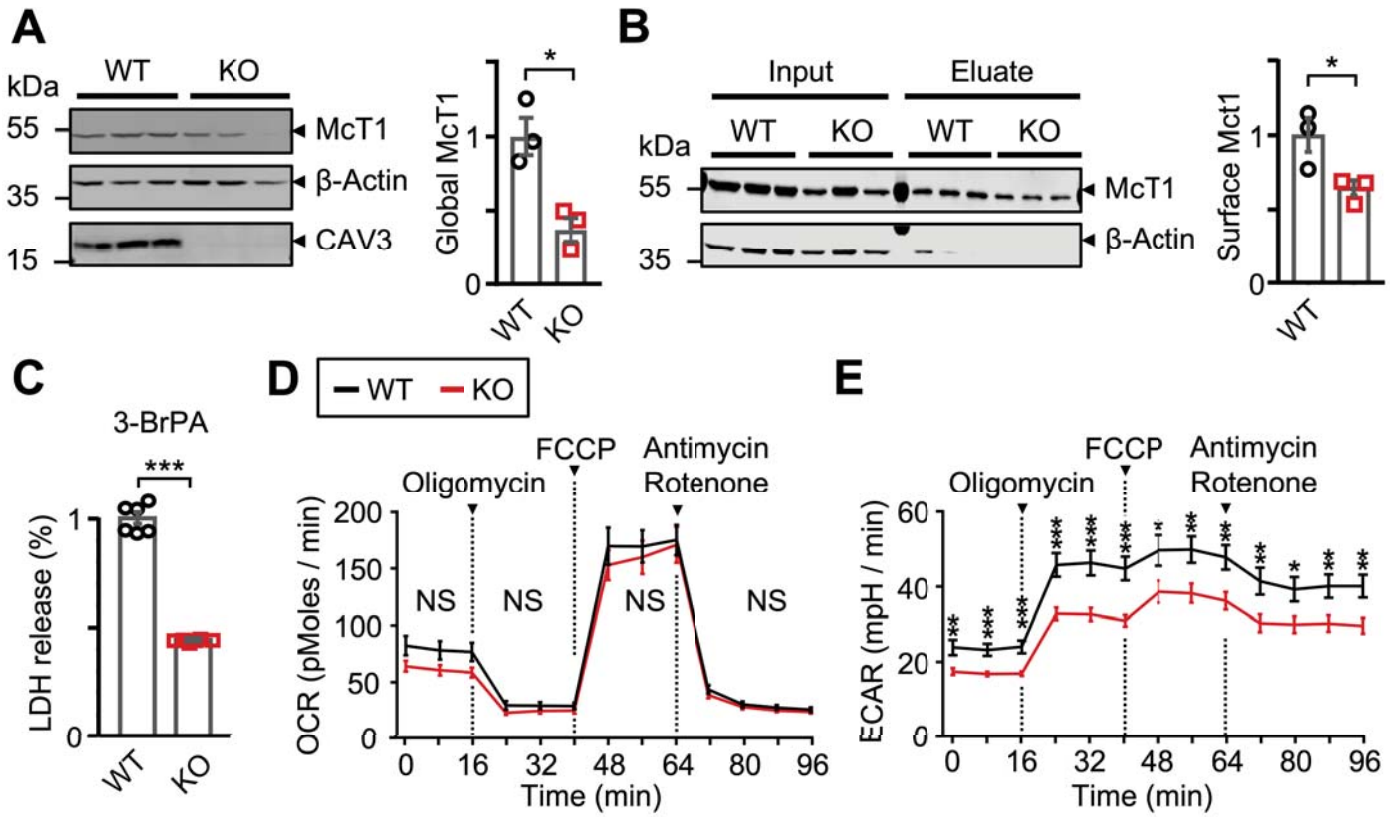
A
kDa
WT
KO
55
35
15
McT1
β-Actin
CAV3
Global McT1
1
0
*
WT
KO
B
Input
Eluate
WT
KO
WT
KO
kDa
55
35
McT1
β-Actin
Surface Mct1
1
0
*
WT
C
3-BrPA
***
LDH release (%)
1
0
WT
KO
D
WT
KO
FCCP
Antimycin
Rotenone
Oligomycin
OCR (pMoles / min)
200
150
100
50
0
NS
NS
NS
NS
0
16
32
48
64
80
96
Time (min)
E
FCCP
Antimycin
Rotenone
Oligomycin
ECAR (mpH / min)
60
40
20
0
0
16
32
48
64
80
96
Time (min)

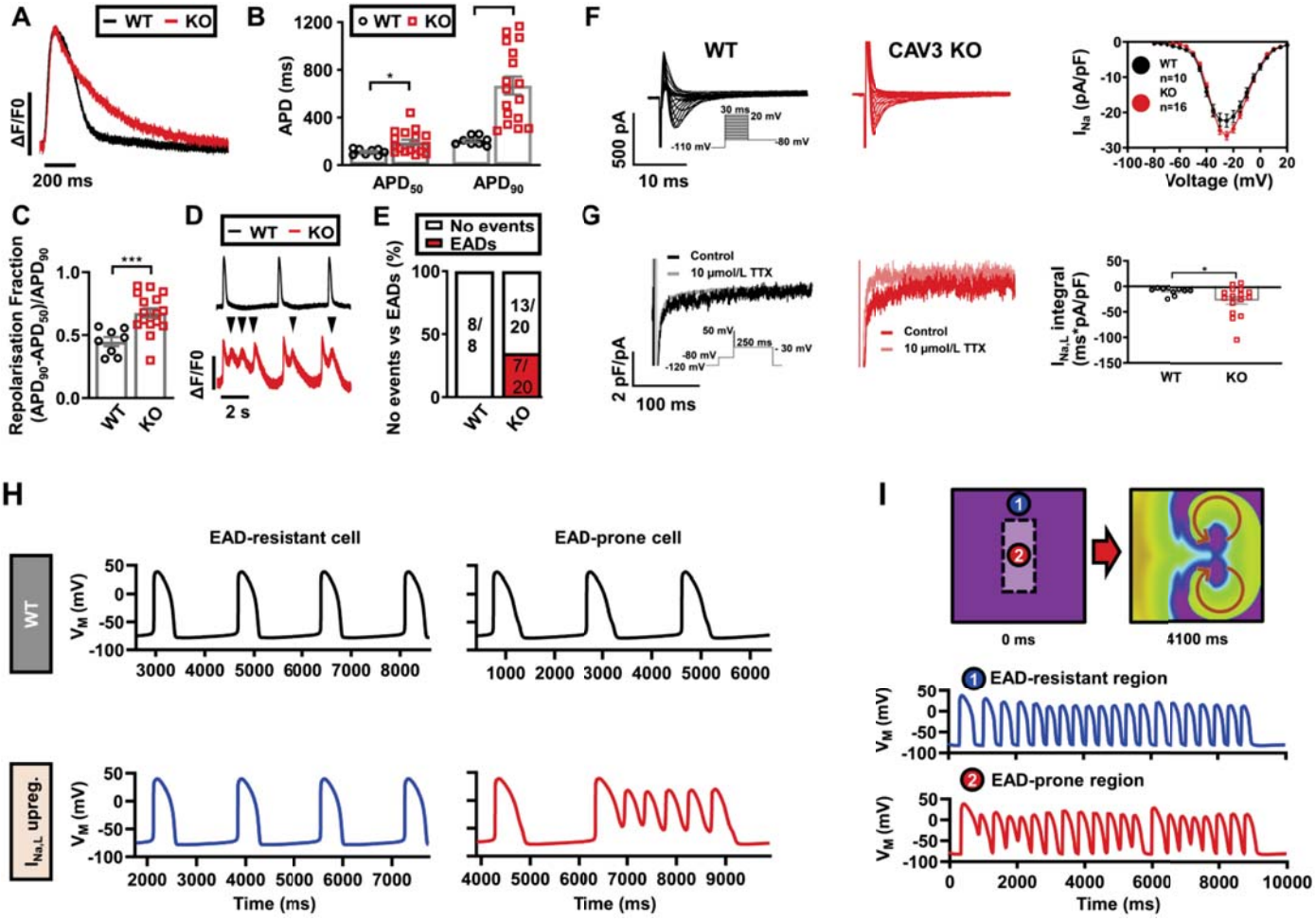
A
WT
KO
ΔF/F0
200 ms
B
WT
KO
APD (ms)
APD50
APD90
C
Repolarisation Fraction
(APD90-APD50)/APD90
WT
KO
D
WT
KO
ΔF/F0
2 s
E
No events
EADs
No events vs EADs (%)
8/8
13/20
7/20
F
WT
CAV3 KO
500 pA
10 ms
-110 mV
30 ms
20 mV
-80 mV
WT n=10
KO n=16
INa (pA/pF)
Voltage (mV)
G
Control
10 µmol/L TTX
2 pF/pA
100 ms
-120 mV
-80 mV
50 mV
250 ms
-30 mV
INa,L integral (ms*pA/pF)
H
EAD-resistant cell
EAD-prone cell
WT
INa,L upreg.
VM (mV)
Time (ms)
I
0 ms
4100 ms
EAD-resistant region
EAD-prone region
VM (mV)
Time (ms)

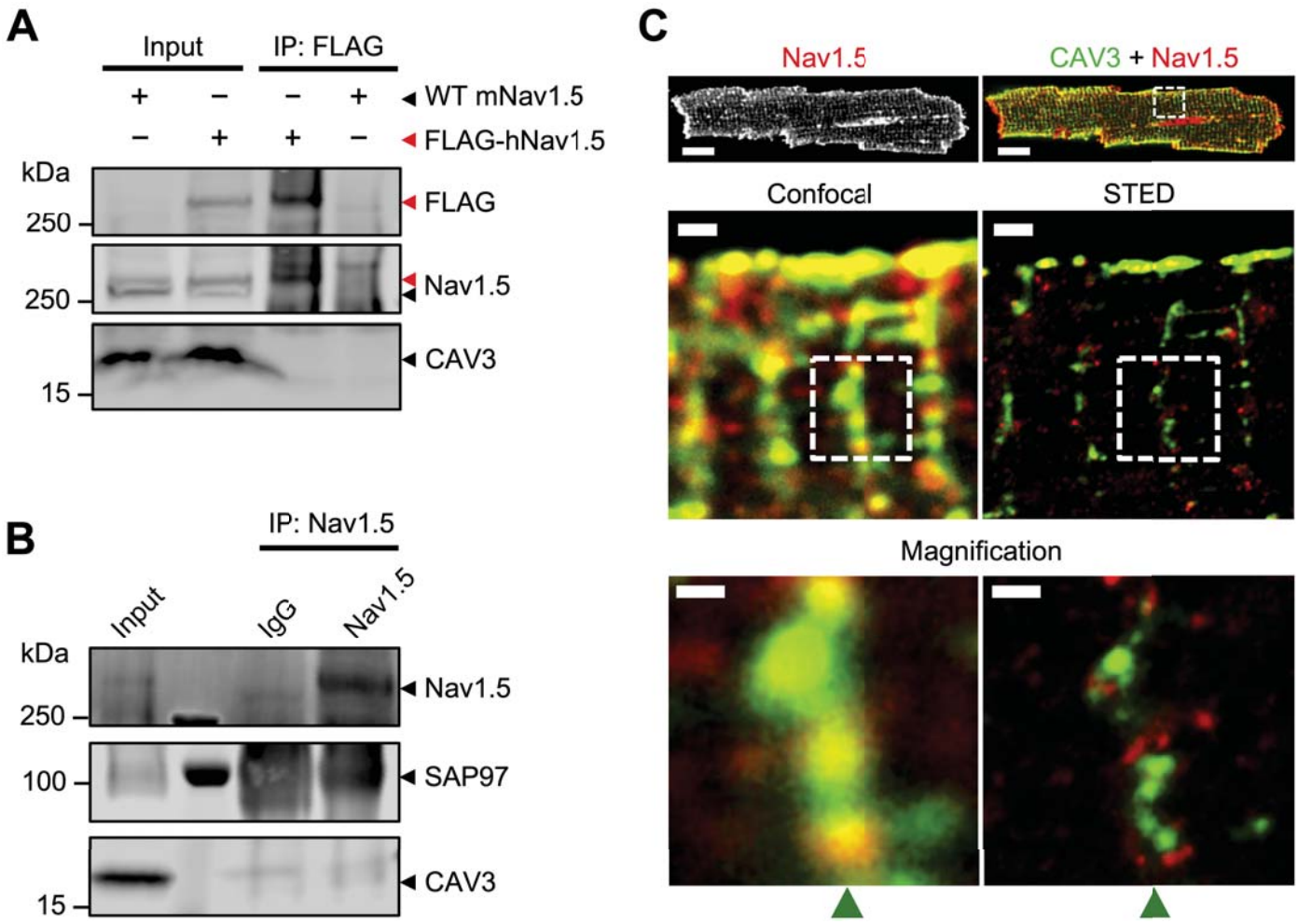
A
Input
IP: FLAG
+ − − + WT mNav1.5
− + + − FLAG-hNav1.5
kDa
250
FLAG
250
Nav1.5
15
CAV3
B
IP: Nav1.5
Input
IgG
Nav1.5
kDa
250
Nav1.5
100
SAP97
15
CAV3
C
Nav1.5
CAV3 + Nav1.5
Confocal
STED
Magnification

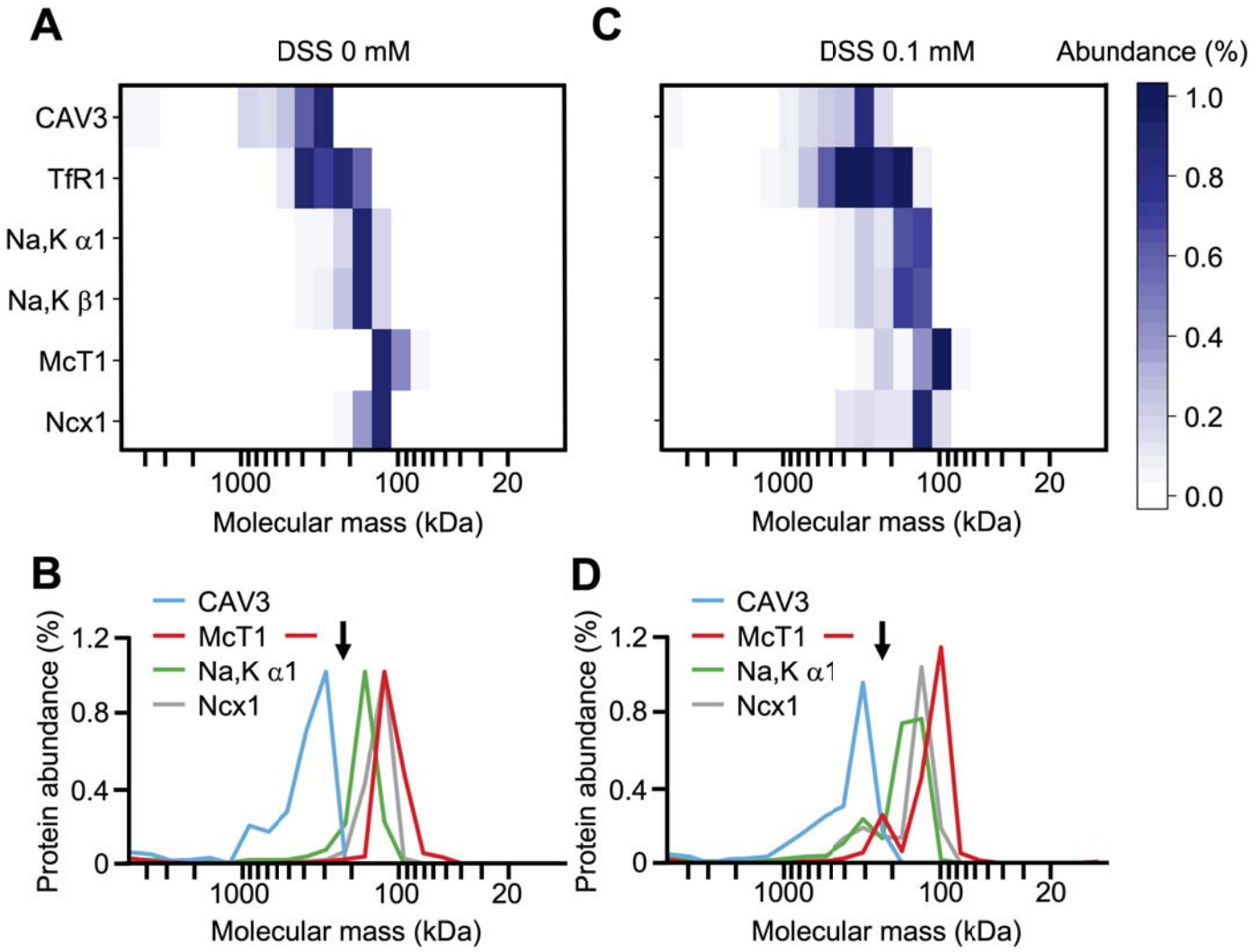
A
DSS 0 mM
CAV3
TfR1
Na,K α1
Na,K β1
McT1
Ncx1
1000
100
20
Molecular mass (kDa)
C
DSS 0.1 mM
Abundance (%)
1.0
0.8
0.6
0.4
0.2
0.0
1000
100
20
Molecular mass (kDa)
B
CAV3
McT1
Na,K α1
Ncx1
Protein abundance (%)
1.2
0.8
0.4
0
1000
100
20
Molecular mass (kDa)
D
CAV3
McT1
Na,K α1
Ncx1
Protein abundance (%)
1.2
0.8
0.4
0
1000
100
20
Molecular mass (kDa)